ScienceDirect®

Mass transfer effects on mucus fluid in the presence of chemical reaction

Padmavathi Thiyagarajan [a] ✉ , Sethamilselvi Sathiamoorthy [a] ✉ , Hemalatha Balasundaram [a] ✉ ,
Oluwole Daniel Makinde [b] ✉ , U. Fernandez-Gamiz [c] ⚲ ✉ , Samad Noeiaghdam [d e] ✉ ,
Shyam Sundar Santra [f] ✉ , Mohamed Altanji [g] ✉

Show more ⌄

:≡ Outline | ⤝ Share ❞ Cite

Get rights and content ↗

Abstract

The mucus fluid vehicle is impacted by the synthetic response that changes the physical science of liquid due to the thickness of the bodily fluid. Additionally, various issues in the respiratory system might happen because of bodily fluid adequacy. A central point of transportation of immunizations to forestall COVID-19 is the concentration level expected during movement, stockpiling, and dispersion. The current review stated that mucus fluid transportation is restrained through magnetic force originating due to heat variation. Permeable channel over respiratory disease and chemicals due to mass reaction–diffusion variation. The bodily fluid development is surveyed by the force, energy, and diffusion condition influence of body powers because of attractive field, source of heat cause of thermal conduction, resistance due to disease chemical reaction cause of concentration profile. The nonlinear arrangement of incomplete differential conditions is addressed by the Laplace transform technique, and MATLAB programming outcomes are initiated for momentum, temperature, and diffusion fields and inferred that the bodily fluid stream decelerates due to magnetic force. The skin friction, Nusselt number, Sherwood number, and the microorganism's thickness are assessed and explained exhaustively. Furthermore, microorganisms are occupied in different elements to survey the mucus fluid mechanism.

Keywords

Chemical reaction; Coronaviruses; Magnetic force; Mass transfer; Mucus fluid; Porosity parameter

---

Nomenclature

g

    Acceleration due to gravity

μ

    Coefficientofviscosity

Kr

    Chemicalreactionparameter

$erfc$

    Complementaryerrorfunction

y

    Coordinateaxisnormaltotheplate

ρ

    Densityofthemucusfluid

θ_m

    Dimensionlesstemperature

t

    Dimensionlesstime

u_m

    Dimensionlessvelocity

M

    HartmannNumber

ν

    Kinematicviscosity

Gm

    MassGrashofnumber

σ^2

PoroaityParameter

Pr

Prandtlnumber

Sc

Schmidnumber

η

Similarityparameter

Gc

SolutalGrashofnumber

x

Spatialcoordinatealongtheplate

Cp

Specificheatatconstantpressure

T

Temperatureofthefluidneartheplate

k

Thermalconductivityofthemucusfluid

Gr

ThermalGrashofnumber

u

Velocityofthemucusfluidinthex $-$ direction

U_0

Velocityoftheplate

β_T

Volumetriccoefficientofthermalexpansion

1. Introduction

We are carrying on with a phenomenal period of vulnerability and risk, which about by SARS-Cov-2 contamination and subsequent COVID-19 disease. Mass exchange is the development of a blend of mass structures from one area to the next. This interaction happens in different businesses to play out a favorable arrangement of cycles like retention, dissipation, refining, etc. This interaction doesn't just

upgrade the productivity of the mucus layer yet additionally decreases the energy commitments for the consistent working of the tissue.

The bodily fluid organ delivers mucous fluid. The construction of physical fluid shifts relying upon its motivation and the region of your body wherein it is found. Every mucus fluid is produced using mucin, a substance that your body produces; however it is generally, 90% of bodily fluid is water. Most of the mucus gel is smooth and precise. Many adults will create somewhere in the range of 1 and 1.5 quarts of bodily fluid daily. Also, most of it is in the respiratory system, which incorporates the mouth, throat, nose, and lungs. Mucous fluid in our lungs can assist with eliminating microorganisms that could make some way or another reason for infection. Mucus in the nose also can help forestall infections, microscopic organisms, and allergens from entering the body.

The respiratory framework is a massive organization of aviation routes whose capacity also simulation of oxygen from breathing in air. The inhalation process is dependent on the diaphragm that creates negative pressure when it drops down and as, a result, the air is sucked towards the alveolus. When the air is breathed in, the $O_2 - CO_2$ trade is done by the alveoli that are available at the finishes of aviation routes in the profound lung locales.

Ordinarily, the bodily fluid layer is approximated as a unique limit condition. In this review, the impacts of high temperature and low stickiness are assessed by mathematically addressing the hotness and mass exchange in two high-to-low scope network areas. Regularly, the main bodily fluid layer is approximated as a powerful limit condition. The one on the miniature size was made for the bodily fluid layer.

Ariane et al., [1] the coefficient of mass transfer (penetrability) of limit layers overall motile cilia are examined through distinct multi-physics. To perceive the primary components of mass transportation happening on the ciliated surface; an explicit operation is sniffed dose in the epithelium of the respiratory tract.

Hina Sadaf and S. Nadeem [2] explored smooth movement produced by cilia and a strain angle in a bent channel. The stream investigation is done within the sight of warm movement and outspread attractive fields. The impacts of a few invigorating boundaries on the stream and warm exchange are concentrated exhaustively with modest Reynolds number approximations.

Unstable one-layered convection of MHD stream because of hotness and mass exchange through a permeable medium limited by a boundless vertical permeable plate is analyzed [3].

Kiskor Kumar Das [4] determined to concentrate on the impact of Dufour on magneto hydrodynamic warmth and mass exchange stream through an increased limitless vertical plate implanted in a porous medium in the presence of synthetic response and hotness sink.

Yao et al., [5] The logical review doesn't present any proof regarding the airborne quality of SARS-Cov-2. Part of Viruses, for example, chickenpox, can be shipped through air current, and don't expect drops

to arrive at the eyes, mouth, or nose. In actuality, SAR-Cov-2 appears to expect drops to arrive, adding its objectives.

Hamida Khatun and Sahin Ahmed [6] examined the occasional mass and hotness vehicle of thin hydromagnetic stream past an explanatory began movement of the endless vertical plate drenched in Darcian permeable system influence of a chemical reaction using the first order.

According to Nilay Atul Kulkarni et al., [7] Vanishing of the bodily fluid layer because of immense temperatures and slight corresponding moistness can be concentrated exhaustively, various energy profiles and neighborhood differences in mucus fluid layer thickness were read up for scopes of extreme basin temperature nature at a delegate stream pace of 20 LPM (liters each moment).

Mubbashar Nazeer et al., [8] investigated two-layered magneto-hydrodynamics of cilia-driven doublet pressure liquid with hotness and mass exchange. Stream elements are planned by utilizing convective limit conditions joined with impacts of gooey dissemination. The underlying phase of airborne viral illness transmission is brought about by infection loaded drops that are produced predominantly by hacking, and sniffling Jayaweeraa et al.,[9].

In [10] planned to exhibit the restricted adequacy of EBD against IAV in the fluid of mucus (sputum). However, we looked to clarify the components liable for this impediment and the circumstances where this restriction happens. Mingkan et al., [11]. The main issue of transportation of vaccinations to hinder COVID-19 is the focus level expected during development, amassing, and scattering.

Riaz et al., [12] the creators fostered the numerical model for entropy generation examination during the peristaltic drive of Jeffrey nanofluids passing in the middle of two unpredictable unbalanced annuli. Entropy propagation brought about by the inevitable impact of hotness and mass exchange of nanofluid and thick dispersal of the considered fluid was appropriated deliberation.

Rajneesh Bhardwaja and Amit Agrawal [13] investigated the drying season of beads launched out from a COVID-19 tainted subject on surfaces of individual assurance hardware (PPE, for example, a facial covering, of numerous drizzles. In other words, extent of drying period of the drop on an ideal superhydrobic surface (direct approach $, \theta \to 180°$) to an ideal hydrophilic surround ($\theta \to 0°$) furthermore the extent of the most limit to least evaporate period of the seep above wall with different connected particle. Inspection gives bits of knowledge that are valuable while planning the PPE to handle the current pandemic situation.

Harshad Sanjay Gaikwad et al., [14] analyzed the vehicle highlights of an impartial solute inserted in a viscoelastic dissolvable over a permeable mini-carrier beneath the joined impacts of enforced pressure inclination and electro osmosis. Under a tissue roof mass exchange limit layer of the liquid or gas, they tackled with the species balance condition utilizing the likeness variable methodology. For a small mass exchange limit layer considered bigger values of Schmidt number to linearize the field of speed.

Heydel et al., [15] utilized a blend of trial ways to deal with distinguish and restrict GST isoforms in olfactory materials, in addition to the nasal bodily fluid. Also, the connection of odorants with GSTs

were concentrated in vitro utilizing a recombinant GST distinguished in both tissue and bodily fluid.

Wenwen Liu et al.,[16] determined protein and metabolite piece of pressure instigated mucus fluid and tissue homogenate to work with a superior comprehension of the course of pressure prompted mucus fluid emission, together with their contribution in natural resistance, alongside the disclosure of novel bioactive mixtures.

Chen Wang et al., [17] air-surface communications of 19 normal private wind toxins with different prospect and authority were checked in a house utilizing quick reaction, spectroscopic strategies and networked mass spectrometric.

The conduct of flimsy MHD stream of Jeffrey liquid over a slanted permeable plate was discussed in [18].

Vasiliki-Georgia Peppa et al., [19] classified the most extreme and least upsides of osmolality that can be recognized in the pleural liquid of patients with various pleural emissions, likely contrasts among them and possible relationships of osmolality with other clinical factors.

Mukherjee and Prasad [20] the force and the hotness move attributes in incompressible electrically directing limit layer stream over a dramatically extending sheet under the impact of attractive field with warm radiation through permeable medium.

Rana et al. [25], [26]intended to hypothesize the actual parts of a (binarychemical reaction)BCR and (Arrhenius activation energy) ACE on magneto hydrodynamics Williamson micro-polar nanofluid course through an upward extending sheet. Also, explored the components of APE result energy, exothermic/endothermic component, it nano-bio-blood delineation property exuding from the dramatically extended surface together with electro-magneto-hydrodynamics.

NagarajuGajjela et al., [29], [30], [31], [32] investigated mixed (combined) convection stagnation point pair stress nanofluid over a stretched cylinder with varying thermal conductivity. In the presence of viscous dissipation and an internal heat source studied for various bio fluids.

Investigated the impression of warm radiation on 2D higher request MHD multiphase liquids stream instead of extending on a plane surface by imagining various substantial impacts.

The present survey expressed that transportation of mucus fluid is limited through attractive power is created because of changes in hotness. Porous channel over respiratory sickness, and dissemination of chemical rebound because of changes in mass. Flow chart of MCC activities given below in Fig. 1a.
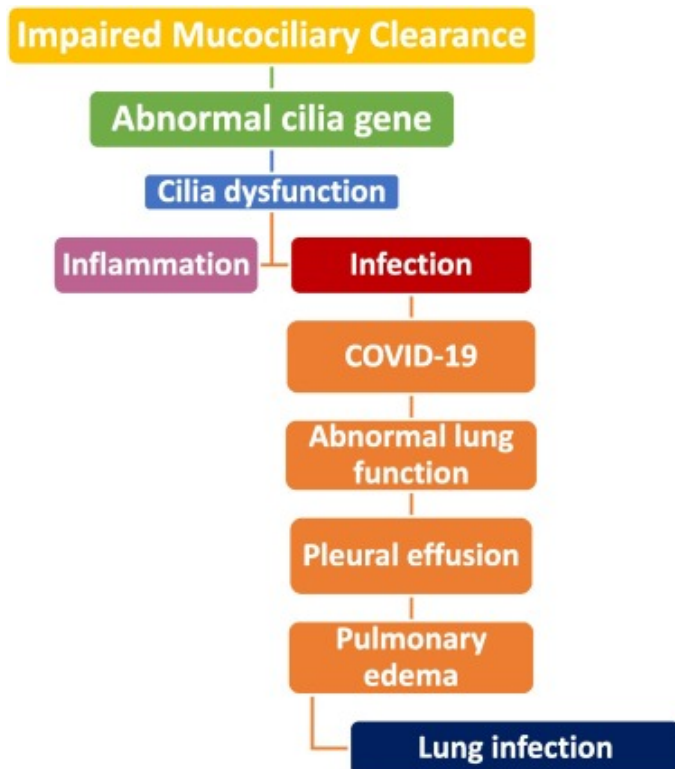
Fig. 1a. Proposed pathogenesis of primary ciliary dyskinesia lung disease.

R. Robinot et al. [27] COVID contamination can cut down the woodlands of hair-like that protect our aviation routes, obliterating an essential obstruction to holding the infection back from housing somewhere down in the lungs. During the virus or bacterial infection respiratory cells are damaged. Hair-like design helps to move mucus fluid. Without this position there is no mucus transportation in the respiratory system.

The advancement of the organic liquid is reviewed by the motion, energy and dispersion condition impact of body force as a result of magnetic field, wellspring of hotness reason for warm conduction, obstruction because of COVID-19 infection compound response reason for fixation field. An examination of the current outcomeswith prior investigations shows great arrangement, in this manner exhibiting the new strategy for the Coronavirus disease. The review finds applications in biochemical response designing cycles, magnetic materials handling, etc.

2. Formulation of the problem

Consider the flimsy one-layered convection stream of an incompressible viscid fluid over a permeable medium limited by an immense perpendicular permeable portion supporting across magnetic force. The physical configuration is shown in Fig. 1.
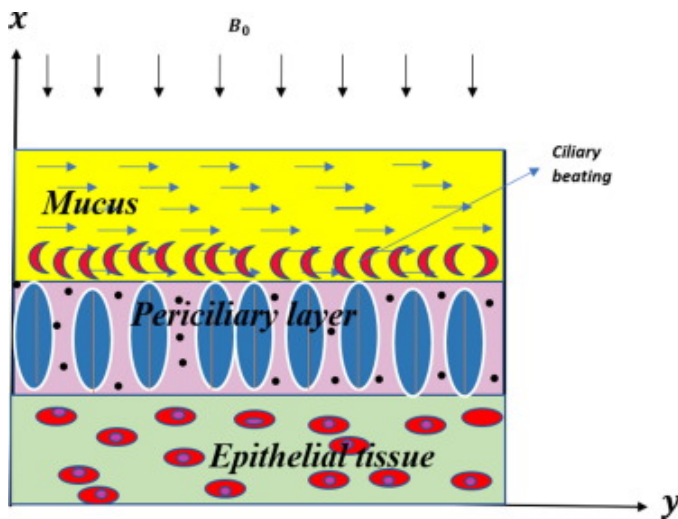
Download : Download high-res image (199KB)

Download : Download full-size image

Fig. 1. Physical configuration of the Mucus layer.

The following assumptions are made;

- The x^*- axis is taken to be the infinite region and the $\& \; y^*-$ axis normal to it.

- Here the velocity components along x^*- axis and y^* y^* axes can be $u_m^* \; and \; v_m^*$ which are chosen in the upward direction along with the plate and normal to the plate respectively.

- A uniform magnetic field force applied perpendicular to the plate.

- At first the plate and the liquid at a similar temperature T_∞^* with concentration level C_∞^* at every level. At time $t^* > 0$, the plate temperature is unexpectedly lifted to T_w^* and concentration level at the plate gets heightened to C_w^* and are kept up with consistent from there on.

- It is expected that the plate is sped up with speed $u_m^* = u_0$ in their unique plane at time $t^* < 0$

With the above presumption and under regular limit layer and <u>Boussinesq's</u> estimation, the overseeing conditions diminish to [4] & [26];

Mass conservation:

$$\frac{\partial v_m^*}{\partial y^*} = 0 \tag{1}$$

Momentum conservation:

$$\frac{\partial u_m^*}{\partial t^*} = -\frac{\partial p_m}{\partial x} + \nu\left(\frac{\partial^2 u_m^*}{\partial y^{*2}}\right) + g\beta_T(T_m^* - T_\infty^*) + g\beta_C(C_m^* - C_\infty^*)$$

$$-\frac{\nu}{k_m^*}u_m^* - \frac{\sigma B_0^2 u_m^*}{\rho} \tag{2}$$

Energy Conservation:

$$\left(\frac{\partial T_m{}^*}{\partial t^*}\right) = \frac{k_T}{\rho C_p}\left(\frac{\partial^2 T_m{}^*}{\partial y^{*2}}\right) \tag{3}$$

Concentration Conservation:

$$\left(\frac{\partial C_m{}^*}{\partial t^*}\right) = D\left(\frac{\partial^2 C_m{}^*}{\partial y^{*2}}\right) - k\left(C_m{}^* - C_\infty{}^*\right) \tag{4}$$

where, $u_m{}^*$ $and v_m{}^*$ are velocity components in the x^* $\& y^*$ direction correspondingly, g represents acceleration due to gravity. $\beta_T \& \beta_C$ are the co-efficient of <u>volumetric</u> expansion with Temperature and Concentration respectively,D represent molecular <u>diffusivity</u>, ν represents <u>kinematic viscosity</u>, σ represents <u>electrical conductivity</u>, $T_m{}^* \& T_\infty{}^*$ are the initial mucus fluid temperature of the fluid at the boundary layer and far from the fluid portion. $C_m{}^*$ $and C_\infty{}^*$ are the initial mucus fluid temperature of the fluid at the boundary layer and far from the fluid portion. k is the co-efficient of chemical reaction, k_T represents <u>thermal conductivity</u>, C_p represents specific heat at constant pressure,B_0 magnetic force parameter, ρ represents density of the mucus fluid,t^* represents time.

Along with introductory and matching conditions are,

$$u_m{}^* = 0 \ and \ T_m{}^* = T_\infty{}^* \ for y^* \geq 0, x^* > 0, t^* \leq 0$$

$$u_m{}^* = u_0 \ and \ T_m{}^* = T_w{}^*, C_m{}^* = C_w{}^* \ at y^* = 0$$

$$u_m{}^* = 0 \ and \ T_m{}^* = T_\infty{}^*, C_m{}^* = C_\infty{}^* \ at y^* \to \infty t > 0 \tag{5}$$

Henceforth non-dimensional quantities are recycled in the current issue to preclude obscure boundary:

$$u_m = \frac{u_m{}^*}{u_0}, = \frac{x^*}{h_p}, y = \frac{y^* U_0}{\nu}, \theta_m{}^* = \frac{T_m{}^* - T_\infty{}^*}{T_w{}^* - T_\infty{}^*}, \tag{6}$$

$$C^* = \frac{C_m{}^* - C_\infty{}^*}{C_w{}^* - C_\infty{}^*}, t = \frac{t^* v_0{}^2}{\nu}, p = \frac{p_m{}^*}{\rho u_0{}^2}$$

where $\theta_m{}^*$, C^* are <u>dimensionless Temperature</u> and Concentration for MucousGel.

Subsequently by utilizing the above dimensionless amounts, the Equations (2), (3), (4) in the non-layered from can be composed as.

<u>Dimensionless governing equation</u>:

$$\frac{\partial u_m}{\partial t} = g + \left(\frac{\partial^2 u_m}{\partial y^2}\right) - \sigma^2 u_m - M u_m + Gr \theta_m + Gc C \tag{7}$$

$$\frac{\partial \theta_m}{\partial t} = \frac{1}{Pr}\frac{\partial^2 \theta_m}{\partial y^2} \tag{8}$$

$$\frac{\partial C}{\partial t} = \frac{1}{Sc}\frac{\partial^2 \theta_m}{\partial y^2} - K_r C \tag{9}$$

where,

$$Gr = \frac{g\beta_T(T_w{}^* - T_\infty{}^*)\nu}{U_0{}^3} \text{ [Grashof number]}; \; Gr = \frac{g\beta_C(C_w{}^* - C_\infty{}^*)\nu}{U_0{}^3} \text{ [Mass Grashof number]};$$

$$\sigma^2 = \frac{\nu^2}{U_0{}^2 K} \text{ [Porosity Parameter]};$$

$$Pr = \frac{\mu C_p}{k_T} \text{ [Prandtl number]}; \; Sc = \frac{\nu}{D} \text{ [Schmidt number]}.$$

$$M = \frac{\sigma B_0{}^2 \mu}{U_0{}^2} \text{ [Hartmann Number]};$$

In the substitution of limit conditions are,

$$u_m = 0 \; as \; y \to \infty$$

$$u_m = 1 \; as \; y \to 0$$

$$\theta_m = 0 \; at \; y \geq 0, \; C = 0 \; at \; y \geq 0 \tag{10}$$

$$\theta_m = 0, C = 0 \; as \; y \to \infty$$

$$\theta_m = 1, C = 1 \; as \; y = 0$$

3. Method of solution

We present Laplace change strategy, which is utilized to settle the consistent coefficient tribute with a broken or hasty inhomogeneous term. The Laplace change is a decent vehicle overall for presenting complex indispensable change strategies inside an effectively reasonable setting. For further work, we need $\eta, F, R, a \, and \, b$ perhaps initiate in the Appendix A.

The arrangements of the equations (7), (8), (9) dependent upon limit condition (10) are as per the following:

$$L\left[\frac{\partial \theta_m}{\partial t}\right] = \frac{1}{Pr} L\left[\frac{\partial^2 \theta_m}{\partial y^2}\right]$$

$$\frac{d^2 \theta_m}{dy^2} - Pr \; S \; L[\theta_m] = 0$$

$$L(\theta_m) = \frac{e^{-y\sqrt{Pr \, S}}}{s} \tag{11}$$

$$L\left[\frac{\partial C_m}{\partial t}\right] = \frac{1}{Sc} L\left[\frac{\partial^2 C_m}{\partial y^2}\right] - K_r \; Sc \; L\,[C]$$

$$\left[\frac{d^2 C_m}{dy^2}\right] - Sc\frac{dC_m}{dt} - K_r \; Sc \; L[C] = 0$$

$$L(C) = \frac{e^{-y\sqrt{Pr(S+K_r)}}}{s} \tag{12}$$

$$L\left[\frac{\partial u_m}{\partial t}\right] = L\left[\frac{\partial^2 u_m}{\partial y^2}\right] + Gr \; L[\theta_m] + Gc \; L[C_m] - L\left[(\sigma^2 + M^2)\right]$$

$$\left[\frac{d^2 u_m}{dy^2}\right] - Sc\frac{dC_m}{dt} - (\sigma^2 + M^2 + S) \; L[u] = Gr \; L(\theta_m) + Gc \; L(C_m)$$

$$L(u_m) \tag{13}$$

$$= \frac{e^{-y\sqrt{s+F}}}{s} - \frac{Gr}{F}\left[\frac{e^{-y\sqrt{s+F}}}{s-a} - \frac{e^{-y\sqrt{s+F}}}{s}\right] + \frac{Gm}{R}\left[\left[\frac{e^{-y\sqrt{s+F}}}{s-b} - \frac{e^{-y\sqrt{s+F}}}{s}\right]\right]$$

$$- \frac{g}{F}\left[\frac{e^{-y\sqrt{s+F}}}{s} - \frac{e^{-y\sqrt{s+F}}}{s-(-F)}\right] + \frac{Gr}{F}\left[\frac{e^{-y\sqrt{Pr\,S}}}{s-a} - \frac{e^{-y\sqrt{Pr\,S}}}{s}\right] - \frac{g}{F}\left[\frac{1}{s} - \frac{1}{s-(-F)}\right]$$

$$+ \frac{Gm}{R}\left[\left[\frac{e^{-y\sqrt{Sc(S+K_r)}}}{s-b} - \frac{e^{-y\sqrt{Sc(S+K_r)}}}{s}\right]\right]$$

catching opposite Laplace-Transforms of the equations (11), (12), (13) the individual fixation, heat and speed profiles are determined as outfitted down.

Inverse Laplace:

$$\theta_m = L^{-1}\left[\frac{e^{-y\sqrt{\Pr S}}}{s}\right]$$

$$\boldsymbol{\theta_m = erfc\left(\eta\sqrt{Pr}\right)} \tag{14}$$

$$\boldsymbol{C_m} = L^{-1}\left[\frac{e^{-y\sqrt{\Pr(S+K_r)}}}{s}\right]$$

$$\boldsymbol{C_m} \tag{15}$$
$$= \tfrac{1}{2}\left\{\left[e^{-y\sqrt{Sc(K_r)}}\left[erfc\left(\eta\sqrt{Sc}\right)-\sqrt{Sc(K_r t)}\right]\right]+\left[e^{y\sqrt{Sc(K_r)}}\left[erfc\left[\left(\eta\sqrt{Sc}\right)+\sqrt{Sc(K_r t)}\right]\right]\right]\right\}$$

$$u_m$$
$$= L^{-1}$$
$$\left[\frac{e^{-y\sqrt{s+F}}}{s} - \frac{Gr}{F}\left[\frac{e^{-y\sqrt{s+F}}}{s-a} - \frac{e^{-y\sqrt{s+F}}}{s}\right]+\frac{Gm}{R}\left[\left[\frac{e^{-y\sqrt{s+F}}}{s-b} - \frac{e^{-y\sqrt{s+F}}}{s}\right]\right]\right]$$
$$-\frac{g}{F}\left[\frac{e^{-y\sqrt{s+F}}}{s} - \frac{e^{-y\sqrt{s+F}}}{s-(-F)}\right]+\frac{Gr}{F}\left[\frac{e^{-y\sqrt{\Pr S}}}{s-a} - \frac{e^{-y\sqrt{\Pr S}}}{s}\right]-\frac{g}{F}\left[\frac{1}{s} - \frac{1}{s-(-F)}\right]+\frac{Gm}{R}\left[\left[\frac{e^{-y\sqrt{Sc(S+K_r)}}}{s-b} - \frac{e^{-y\sqrt{Sc(S+K_r)}}}{s}\right]\right]\right]$$

$$\tag{16}$$

$$\boldsymbol{u_m} = \tfrac{1}{2}\left\{\left[e^{-y\sqrt{F}}[erfc[(\eta)-\sqrt{Ft}]]\right]+\left[e^{y\sqrt{F}}[erfc[(\eta)+\sqrt{Ft}]]\right]\right\}$$
$$-\left(\frac{Gr}{F}\right)\left(\frac{e^{at}}{2}\right)\left\{\left[e^{-y\sqrt{a+F}}\left[erfc\left[(\eta)-\sqrt{(a+F)t}\right]\right]\right]+\left[e^{y\sqrt{a+F}}\left[erfc\left[(\eta)+\sqrt{(a+F)t}\right]\right]\right]\right\}$$
$$+\left(\frac{Gr}{F}\right)\left(\frac{e^{bt}}{2}\right)\left\{\left[e^{-y\sqrt{F}}[erfc[(\eta)-\sqrt{Ft}]]\right]+\left[e^{y\sqrt{F}}[erfc[(\eta)+\sqrt{Ft}]]\right]\right\}$$
$$-\left(\frac{Gm}{R}\right)\left(\frac{e^{bt}}{2}\right)\left\{\left[e^{-y\sqrt{b+F}}\left[erfc\left[(\eta)-\sqrt{(b+F)t}\right]\right]\right]+\left[e^{y\sqrt{b+F}}\left[erfc\left[(\eta)+\sqrt{(b+F)t}\right]\right]\right]\right\}$$
$$+\left(\frac{Gm}{R}\right)\left(\frac{1}{2}\right)\left\{\left[e^{-y\sqrt{F}}[erfc[(\eta)-\sqrt{Ft}]]\right]+\left[e^{y\sqrt{F}}[erfc[(\eta)+\sqrt{Ft}]]\right]\right\}$$
$$+\left(\frac{Gr}{F}\right)\left(\frac{e^{at}}{2}\right)\left\{\left[e^{-y\sqrt{\Pr(a)}}\left[erfc(\eta\sqrt{Pr})-\sqrt{(at)}\right]\right]+\left[e^{y\sqrt{\Pr(a)}}\left[erfc(\eta\sqrt{Pr})+\sqrt{(at)}\right]\right]\right\}$$
$$-\left(\frac{Gr}{F}\right)\left\{erfc(\eta\sqrt{Pr})\right\}$$
$$+\left(\frac{Gm}{R}\right)\left(\frac{e^{bt}}{2}\right.$$
$$\left.\right)\left\{\left[e^{-y\sqrt{Sc(b+K_r)}}\left[erfc\left[\left(\eta\sqrt{Sc}\right)-\sqrt{(b+K_r)t}\right]\right]\right]+\left[e^{y\sqrt{Sc(b+K_r)}}\left[erfc\left[\left(\eta\sqrt{Sc}\right)+\sqrt{(b+K_r)t}\right]\right]\right]\right\}$$
$$-\left(\frac{Gm}{R}\right)\left(\frac{1}{2}\right)\left\{\left[e^{-y\sqrt{Sc(K_r)}}\left[erfc\left[\left(\eta\sqrt{Sc}\right)-\sqrt{(K_r)t}\right]\right]\right]+\left[e^{-y\sqrt{Sc(K_r)}}\left[erfc\left[\left(\eta\sqrt{Sc}\right)-\sqrt{(K_r)t}\right]\right]\right]\right\}$$
$$-\left(\frac{g}{F}\right)\left(\frac{e^{-Ft}}{2}\right)\{2erfc(\eta)\}$$
$$-\left(\frac{g}{F}\right)\left(\frac{1}{2}\right)\left\{\left[e^{-y\sqrt{F}}[erfc[(\eta)-\sqrt{Ft}]]\right]+\left[e^{y\sqrt{F}}[erfc[(\eta)+\sqrt{Ft}]]\right]\right\}-\left(\frac{g}{F}\right)$$
$$+\left(\frac{g}{F}\right)\left(e^{-Ft}\right)$$

Skin Friction:

Realizing the momentum distribution, we presently concentrate on the progressions in the skin friction. Hence the <u>wall shear stress</u> in the presence of chemical reaction field is obsessed by,

$$\tau = \left[\frac{\partial u_m}{\partial y}\right]_{y=0} = \left[\frac{\partial u_m}{\partial \eta}\right]_{\eta=0}$$

$$= \frac{e^{-Ft}g}{2F\sqrt{t}} - \frac{e^{at}\,\mathrm{Gr}\left(\mathrm{erfc}\left[-\sqrt{(a+F)t}\right]+\mathrm{erfc}\left[\sqrt{(a+F)t}\right]\right)}{4F\sqrt{t}} + \frac{e^{bt}\,\mathrm{Gr}\left(\mathrm{erfc}\left[-\sqrt{Ft}\right]+\mathrm{erfc}\left[\sqrt{Ft}\right]\right)}{4F\sqrt{t}}$$

$$- \frac{e^{bt}\,\mathrm{Gm}\left(\mathrm{erfc}\left[-\sqrt{(b+F)t}\right]+\mathrm{Erfc}\left[\sqrt{(b+F)t}\right]\right)}{4R\sqrt{t}} + \frac{\mathrm{Gm}\left(\mathrm{erfc}\left[-\sqrt{Ft}\right]+\mathrm{Erfc}\left[\sqrt{Ft}\right]\right)}{4R\sqrt{t}}$$

$$+ \frac{e^{at}\,\mathrm{Gr}\left(\mathrm{erfc}\left[-\sqrt{at}\right]+\mathrm{erfc}\left[\sqrt{at}\right]\right)}{4F\sqrt{t}} - \frac{\mathrm{Gr}}{2F\sqrt{t}} + \frac{e^{bt}\,\mathrm{Gm}\left(\mathrm{erfc}\left[-\sqrt{t(b+K_r)}\right]+\mathrm{erfc}\left[\sqrt{t(b+K_r)}\right]\right)}{4R\sqrt{t}}$$

$$- \frac{\mathrm{Gm}\left(\mathrm{erfc}\left[-\sqrt{tK_r}\right]+\mathrm{erfc}\left[\sqrt{tK_r}\right]\right)}{4R\sqrt{t}} - \frac{e^{-Ft}g}{2F\sqrt{t}} - \frac{g\left(\mathrm{erfc}\left[-\sqrt{Ft}\right]+\mathrm{erfc}\left[\sqrt{Ft}\right]\right)}{4F\sqrt{t}} - \frac{g}{2F\sqrt{t}} + \frac{e^{-Ft}g}{2F\sqrt{t}}$$

<u>Nusselt Number</u>:

In distinct to <u>Temperature distribution</u>, the Nusselt number which is yielded non-layered structure as follows:

$$Nu = \left[\frac{\partial \theta_m}{\partial y}\right]_{y=0} = \left[\frac{\partial \theta_m}{\partial \eta}\right]_{\eta=0} = \frac{\sqrt{\mathrm{Pr}}}{\sqrt{\pi}\sqrt{t}}$$

Sherwood Number:

In distinct to Concentration distribution, Sherwood Number which is yielded non - layered structure as follows.

$$Sh = \left[\frac{\partial C_m}{\partial y}\right]_{y=0} = \left[\frac{\partial C_m}{\partial \eta}\right]_{\eta=0} = \frac{2e^{-K_r \mathrm{Sc}t}\sqrt{\mathrm{sc}}}{\sqrt{\pi}} + \frac{e^{-K_r \mathrm{Sc}t}\sqrt{\mathrm{sc}}}{2\sqrt{\pi}\sqrt{t}} + \frac{1}{2}\sqrt{K_r \mathrm{Sc}}$$

$$\mathrm{erfc}\left[\sqrt{K_r \mathrm{Sc}\,t}\right] + 2\sqrt{K_r\,\mathrm{Sc}}\sqrt{t}\,\mathrm{erfc}\left[\sqrt{K_r\,\mathrm{Sc}\,t}\right]$$

4. Results & discussion

To have an actual perspective on the issue, non-layered momentum distribution, <u>temperature distribution</u>, concentration distributions registered at the plate for various boundaries included and these qualities have been shown in figures.

The upsides of the Prandtl number Pr are picked as 0.71 and 7.0 to address air and water individually. The upsides of Schmidt number Sc are decided to address the presence of different species like Oxygen $Sc = 1.25$, Water $Sc = 1.6$, Carbon dioxide $Sc = 0.94$, Water fume $Sc = 0.60$ and hydrogen $Sc = 0.30$. The upsides of different boundaries are picked erratic.

Whereas some outer power, tension might be held and lead to variety, and it very well may be utilized to modify two indeterminant energies, specifically dynamic and potential. Besides, this is known as the "primary law of thermodynamics". Whenever the strain contrast is under 1 speed, the liquid is expanded. At the point when the strain contrast is $(p << 1)$), diminishing speed profiles are started. Previous numerical investigations have been presented in Table 1.

Table 1. Previous numerical investigations have been presented.

SL No	Author	Research area	Properties of fluid	Non-dimensional parameters	Solution Methodology	Physical parameter
1.	BMJ Rana et al. [25], [26]	3,7,9,14,17	Williamson micropolar nanofluid	$\delta, N_t, E, \Gamma, \gamma, \Omega, N_b, \Lambda, L_e$	EMDM	$C_f = \left[(1+\eta\theta + \Gamma) \left\{ \frac{\partial U}{\partial Y} + \omega \left(\frac{\partial U}{\partial Y} \right)^2 + SN \right\} \right]_{Y=}$
2.	Ariane et al., [1]	7,8	SPH and MSM	D, f, s, Pe, Sh, λ	(DMP)	$Sh = \frac{D_{pcl}}{D}, Pe = \frac{S^2 f}{D}, \lambda = \frac{s}{L_{pcl}}$
3.	Hina Sadaf and S. Nadeem[2]	9,10	Newtonian fluid	$Re, M, Gr, k, Q, \epsilon, \alpha, B, \frac{dp}{dx},$	Numerical method	$Q = F + 2, \Delta p = \int_0^1 \frac{dp}{dx} dx, C_1 = -\frac{1+Bhk}{\log\left[\frac{-h+k}{h+k}\right]}, \quad C_2 = \frac{Bh^2 - 2Bhk + Bk^2}{4} + \frac{\log[(-h+k)(1+Bhk)]}{\log\left[\frac{-h+k}{k+h}\right]}, \quad A, 1$
4.	M.H. Kamel	3,7,11,12	incompressible viscous fluid	$Gm, Gr, Sc, p, K, \eta, M$	Laplace transform	−
5.	Nilay Atul Kulkarnia, ClementKleinstreuer [7]	7,9,14	Mucuc fluid	$Re, Sh, Sc, Sc_t, P,$	CFD	$\frac{d(m_v)}{dt} = A_s \rho D_{av} Sh \left[\frac{(Y_s - Y_a)}{(1 - Y_s)} \right], Y_s = \frac{(W_{liq} P_{sat})}{(W_{liq} P_{sat} - W_{vap}(P_G - P_{sat}))}$

SL No	Author	Research area	Properties of fluid	Non-dimensional parameters	Solution Methodology	Physical parameter
6.	N. Ali et al, [9]	4,15,16	Persitaltic Newtonian fluid,Ellis model	$Re, P, S, \beta,$ F_{ek}, μ_r, α	Bi-section method	$\Delta P = 16\mu_r$ $\int_0^\lambda \left\{ \dfrac{\frac{1}{2}(U_E-1)(k^2-R_1{}^2+R_0{}^2)+\frac{1}{16\mu_r}P_0(k^2-1)^2}{(R_1{}^2-R_0{}^2)^2} \right\} dz$ $Q = \frac{1}{T_p}Q_S dt = q + \left(1 + \frac{\phi^2}{2}\right)$
7.	Nagaraju Gajjela and Mahesh Garvandha [29]	3,5,7,8,11,18	stagnation-point couple stress nanofluid	$Re, \gamma, s, Pr,$ $Sc, ANb,$ $Nt, Ec, Q,$ $Na, Na, \lambda,$ $\varepsilon,$ $h_f h_\theta, h_\phi$ and h	BVPh2.0	$\frac{1}{2}C_f\sqrt{Re_z} = -f''(0)$ $\frac{Nu_z}{\sqrt{Re_z}} = -\left\{1 + \frac{\varepsilon\theta(0)}{1+\varepsilon\theta(0)}\right\}\theta'(0)$ $\frac{Sh_z}{\sqrt{Re_z}} = -\phi'(0)$

1. Bio-convection, 2. Steady flow, 3. MHD, 4. Blood Flow, 5. Chemical reaction, 6. Heat absorption, 7. Heat Transfer, 8. Radial magnetic field, 9. Bio fluid dynamics, 10. Nano fluid, 11. Porous medium, 12. Infinite vertical plate, 13. Cilia, 14. CFD, 15. Swimming micro-organism, 16. Polymer processing flows, 17. Thermal engineering, 18.HAM.

As previously stated, one of the most important tasks of the nasal and lung airways is airway humidification, which is responsible for raising the relative humidity of the air to 100%. Evaporation from the mucus layers that line the airway walls throughout the organ achieves action.

The mucus layer is 95–99 %, as explained previously. By the time the air reaches the alveoli, water evaporation from the mucus layer has humidified the air to nearly 100% relative humidity. The vapor pressure governs the evaporation process while the temperature is below boiling. The capacity of air to contain water vapor increases as its temperature is raised; similarly, the evaporation rate rises as the temperature of the breathed air rises.

Grashof number: The proportion between the lightness force because of spatial variety in liquid thickness (brought about by temperature variation) to the limiting power due to the viscosity of the liquid. Fig. 2, Fig. 2a and Fig. 3, Fig. 3a demonstrates that the velocity dispersions are expanded enthusiastically in order to impact of different expanding Grashof Numbers. This kind of elements

happened in the human respiratory system because of lightness force. This signifies that raisimgbuoyant force raises the body's temperature. Cilia make the mucus fluid to float in the mucociliary layer due to high thickness.
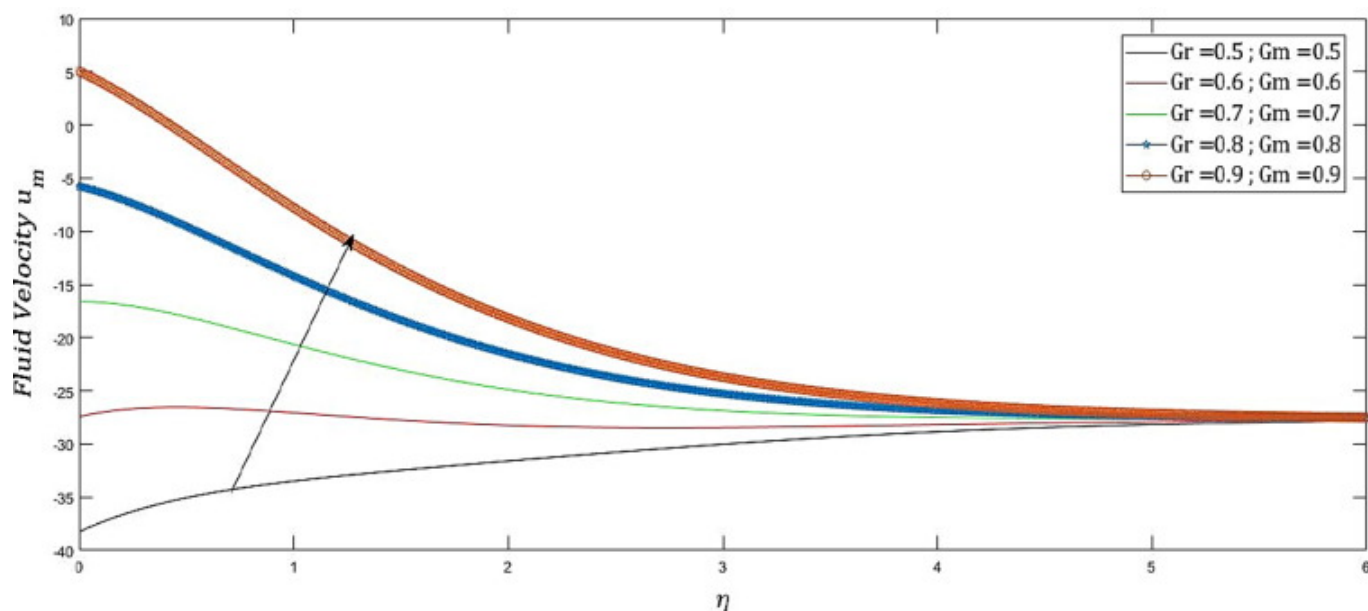
Download : Download high-res image (257KB)

Download : Download full-size image

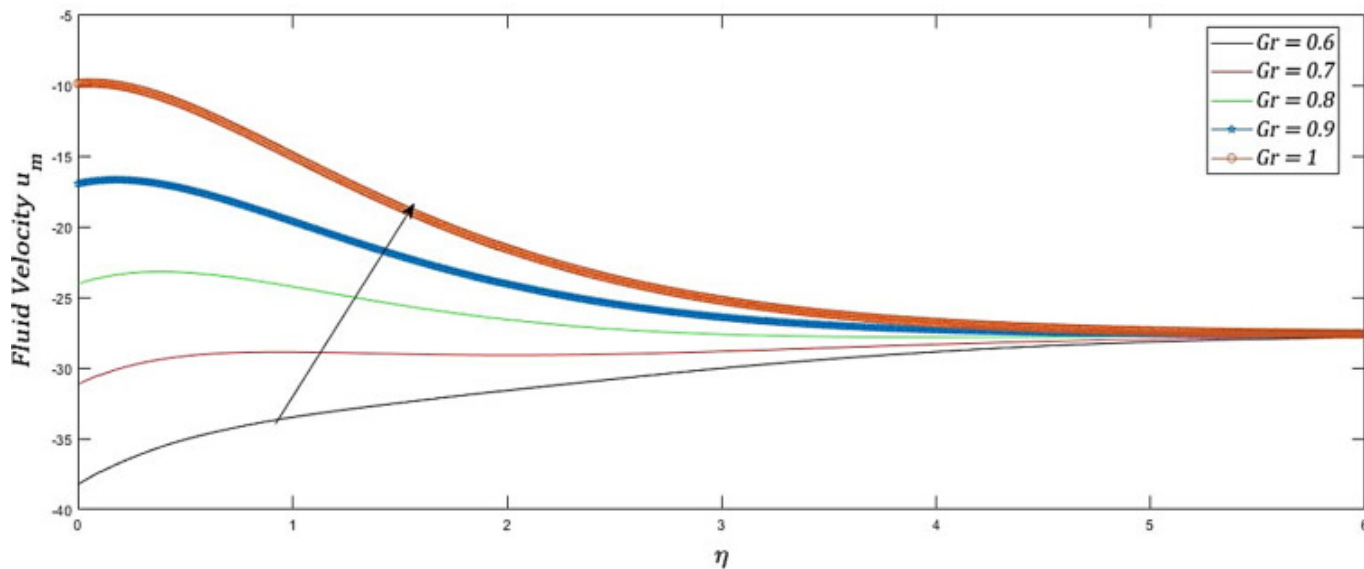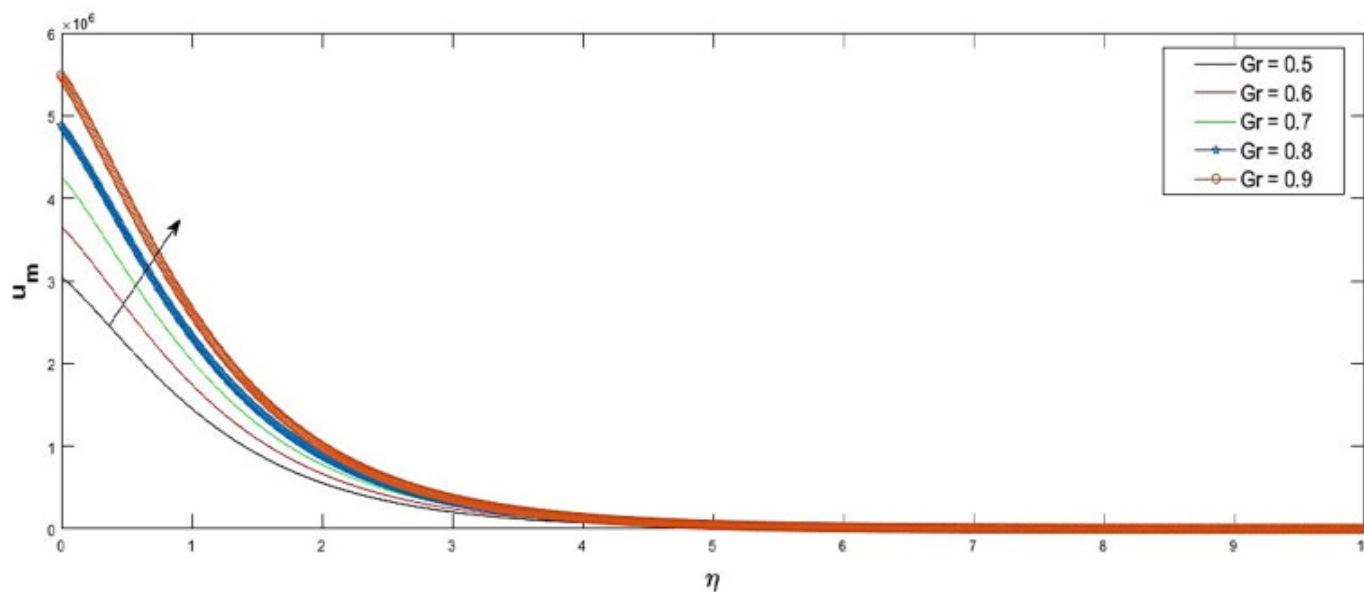Fig. 2. Variation in Velocity profile with respect to mass Grashof number for permeable walls.
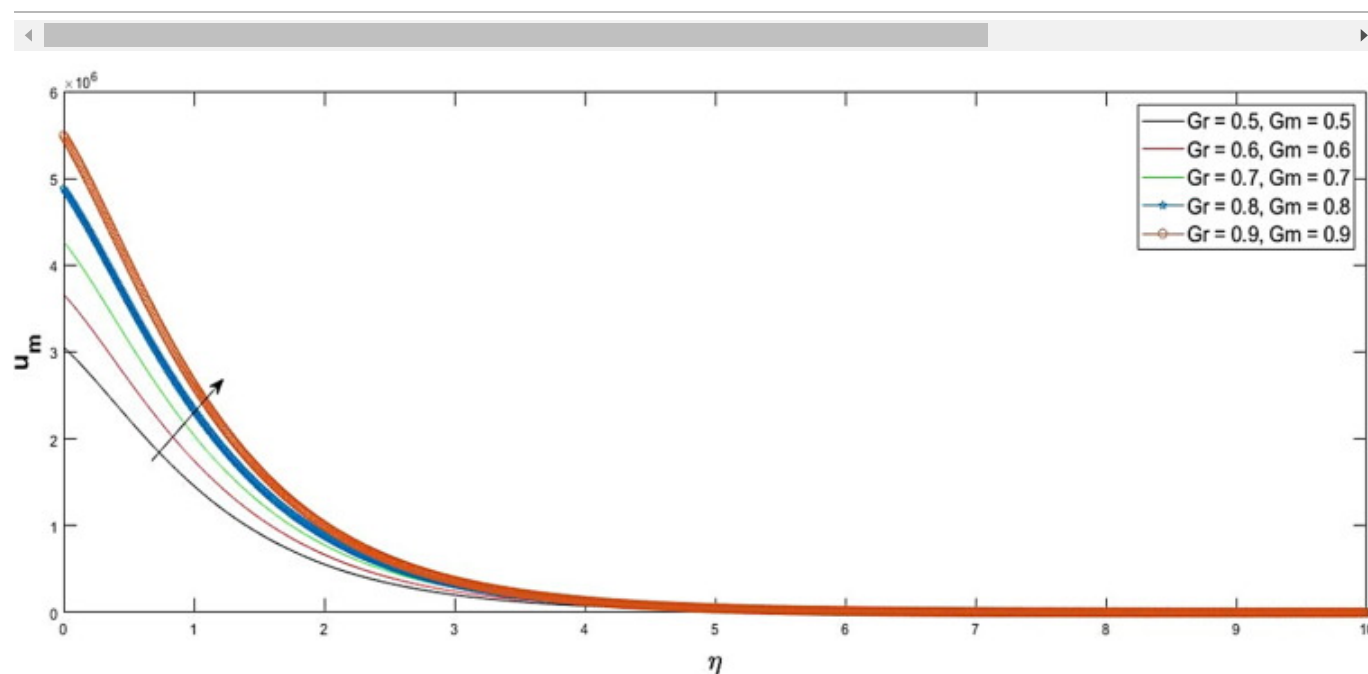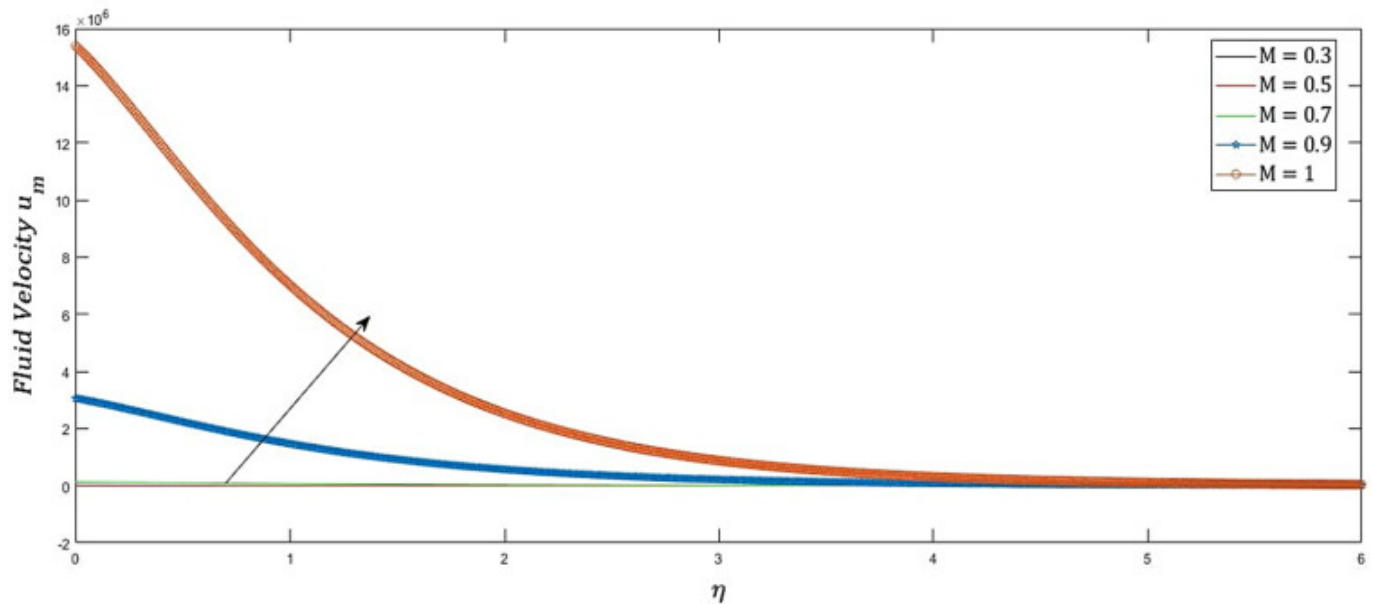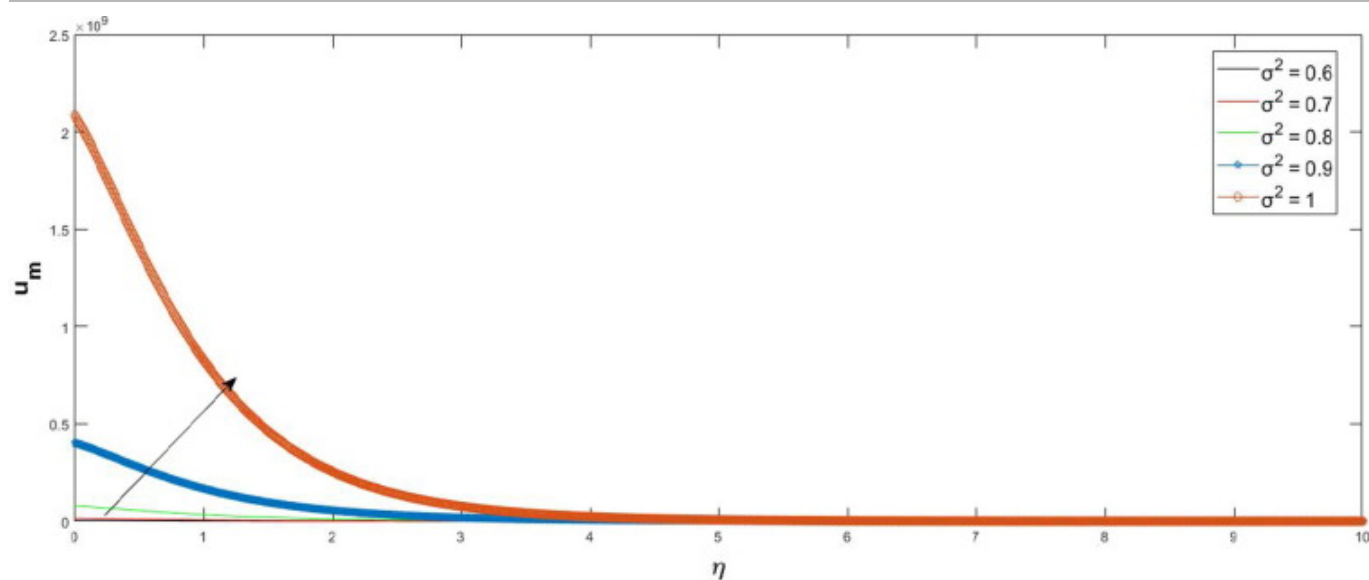

Download : Download high-res image (192KB)

Download : Download full-size image

Fig. 2a. Variation in Velocity profile with respect to mass Grashof number for impermeable walls.

Fig. 3. Variation in Velocity profile with respect to Grashof number for permeable walls.

Fig. 3a. Variation in Velocity profile with respect to Grashof number for impermeable walls.

Hartmann number:

The performance of the Hartmann number is introduced in Fig. 4 & Fig. 4a by expanding the power of the mucus liquid's attractive field energy bit by bit increases in the focal point of the medium. Thus, enlarging moving is contributed by the rise of Lorentz force acting in the cross over course, which obstruct the stream. It is seen that the speed profiles degenerate to zero dynamically for more limited

outstrips from the chamber surface. Accordingly, the solid hindering impact of attractive field is, therefore, distinct.

Download : Download high-res image (183KB)

Download : Download full-size image

Fig. 4. Variation in Velocity profile with respect to Hartmann number for Permeable walls.
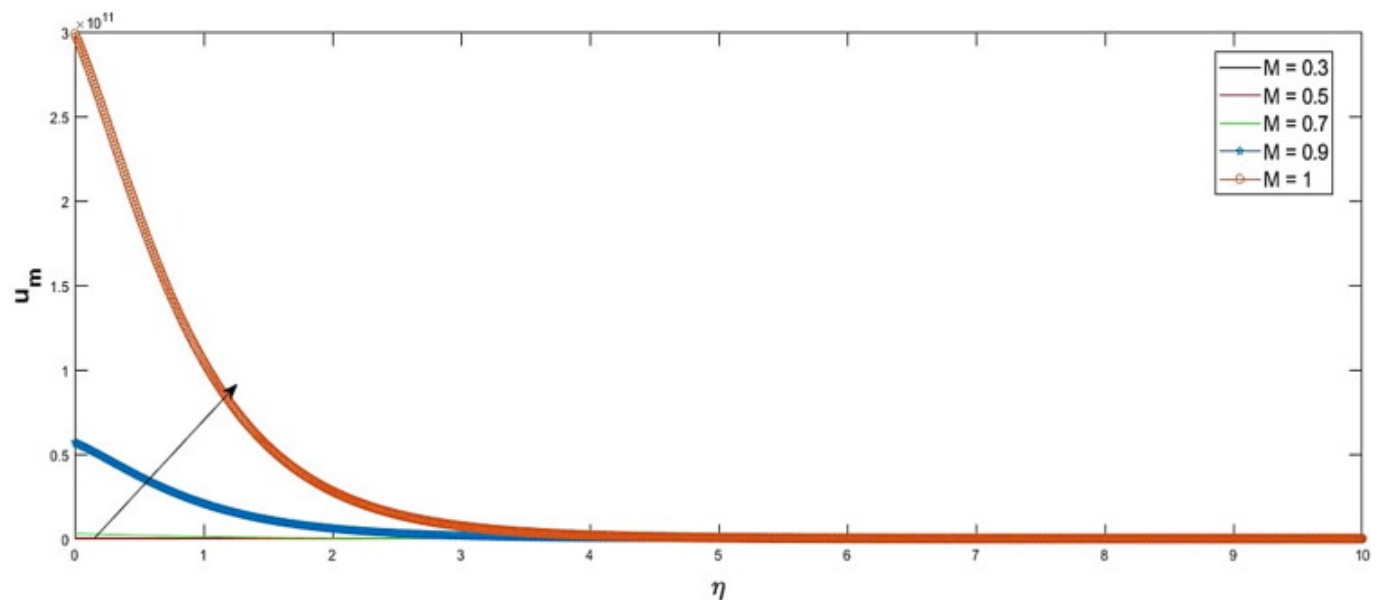
Download : Download high-res image (147KB)

Download : Download full-size image

Fig. 4a. Variation in Velocity profile with respect to Hartmann number for impermeable walls.

Porosity: Fig. 5 intriguing to see that up to a specific time speed of mucus fluid increments and afterward time expected to achieves a consistent state is unprejudiced concerning the worth of

porosity. The scope of lung pores lies between (0 to 1). It might vacillate by time, and it very well may be assessed through arrived at the midpoint of time. If the absence of permeability lack of mucus transport happen in the respiratory system. It shows in the following figure Fig. 2a, Fig. 3a, Fig. 4a.

Download : Download high-res image (149KB)

Download : Download full-size image

Fig. 5. Variation in Velocity profile with respect to Porosity parameter for permeable wall.

Prandtl number:

Fig. 6 shows that the impact of hotness energy is moved through the respiratory system. As the aviation route tissue involves a high measure of water, the bodily fluid and tissue layers are accepted to have a uniform thermodynamic property equivalent to water, which is recommended by Wu et al., [21]&MehdiStitia et al., [22] Dissipation of the fluid (bodily fluid or spit) is generally because of convection over the air-fluid point of interaction, meanwhile the density of the fluid just influences the warm obstruction of the conduction. Currently, the density of the salivation in the oral pit is excluded. Convective hotness move coefficient plays out a crucial job in the free convection inside the human lungs in regards to the effect of COVID-19. The honorable gases (generally likewise the latent gases; some of the time alluded to as aerogens) make up a class of synthetic components with comparative properties; under standard circumstances, they are unscented, dismal, monatomic gases with extremely low substance reactivity. Around 0.16–0.7 for mixtures of noble gases. Noble gases are exceptionally inert aside from when under specific outrageous circumstances. The dormancy of these gases makes them entirely appropriate in applications where responses are not needed. Fig. 6 and Fig. 7 represents that the impact of speed field is raised for the various expanding Pr, time dimensionless boundaries by [23]. In laminar boundary layers, the proportion of the warm to energy limit layer thickness over a level plate is very much approximated by $0.6 < Pr < 50$ [28]. The Prandtl quantities of gases are around 1, which shows that both force and intensity scatter through the liquid at about a similar rate. Heat diffuses rapidly in fluid particles $(Pr \ll 1)$ and gradually in lube $(Pr \gg 1)$
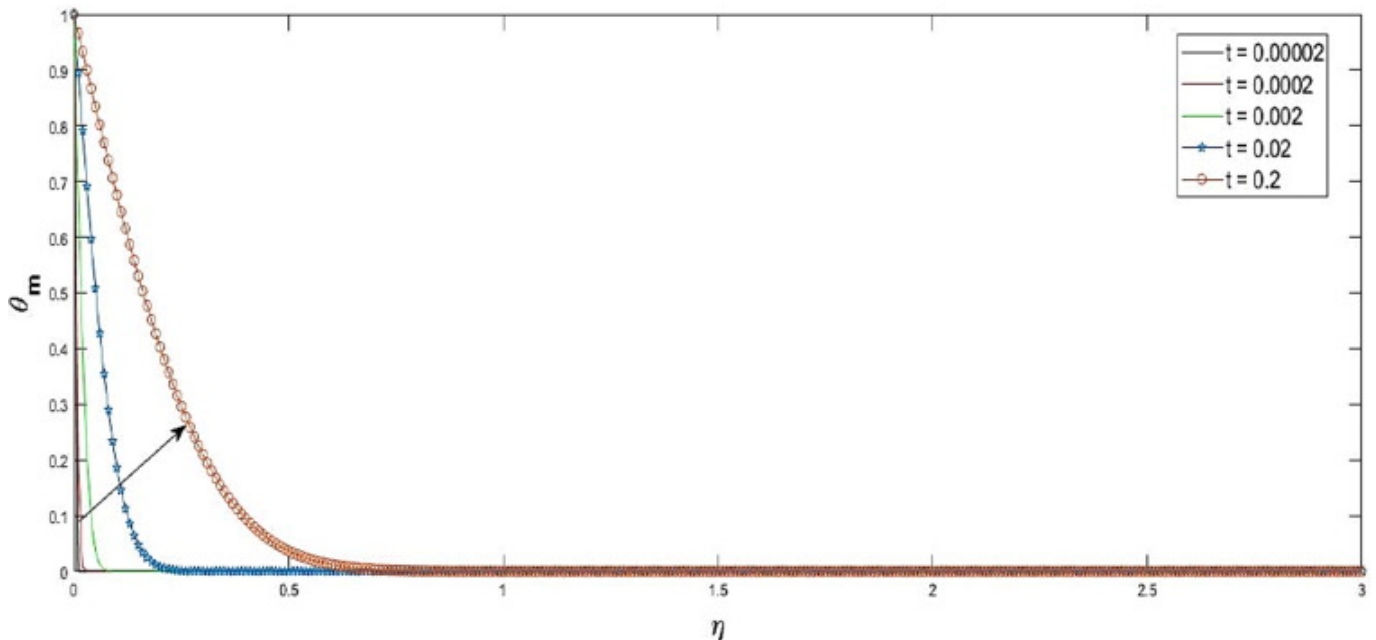
comparative with energy. Therefore, warm limit layer is a lot thicker for fluid metals and a lot slenderer for lubes comparative with speed limit layer.
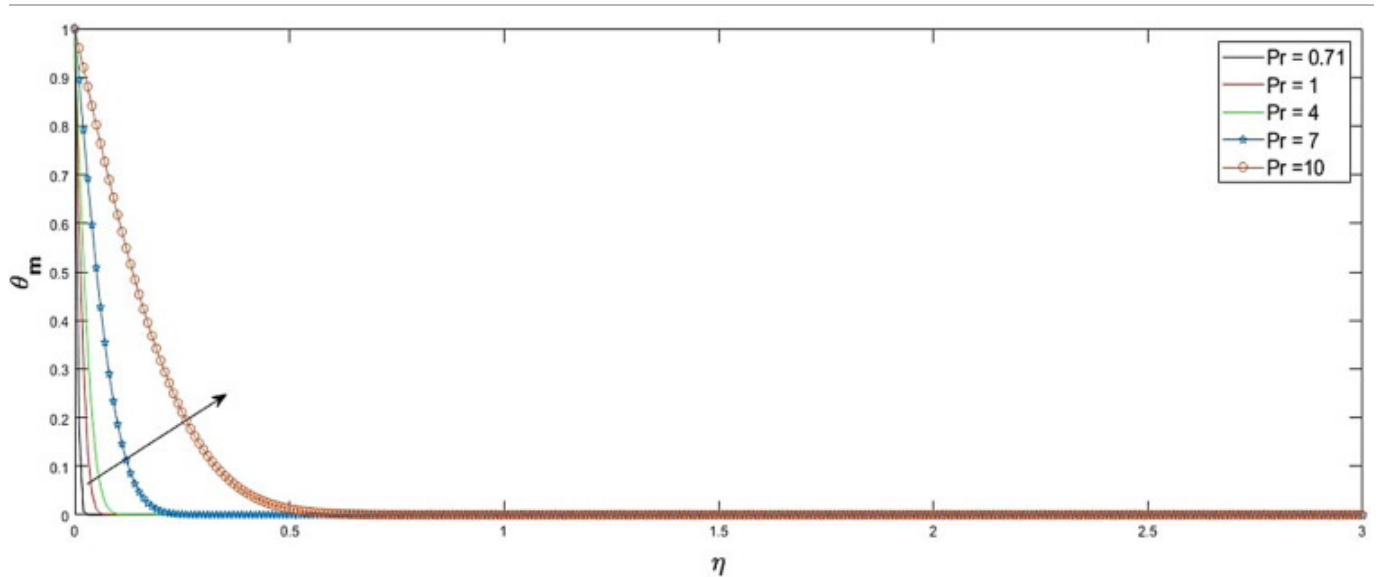
Fig. 6. Variation in Temperature profile with respect to Prandtl Number.

Fig. 7. Variation in Temperature profile with respect to time.

Obviously, such a solution cannot capture the impact of the molecular Prandtl, particularly if Pr is given by a single value, and is thus ineffective. Pr values range from 0.1 to 1, with 0.6 being the most

prevalent (Sagaut, 2006).

Out of 26 (and perhaps more) non-Newtonian liquids, this Prandtl liquid is one of the pseudoplastic visco-inelastic liquids.

Schmidt number:

In this part, we examine the concentration distribution against various factors in Fig. 8 The portion among energy and diffusivity of mass depicts the Schmidt number. The number thickness of minuscule size dust particles diminishes across the channel when Schmidt number (Sc) is upgraded, as displayed in Fig. 8 Higher attractive field brings about the reduction of concentration of particles in Fig. 8 Small fluid particles move from the district of higher focus to a locale of lower concentration, separately.by ↗ Padmavathi and Senthamilselvi [23].
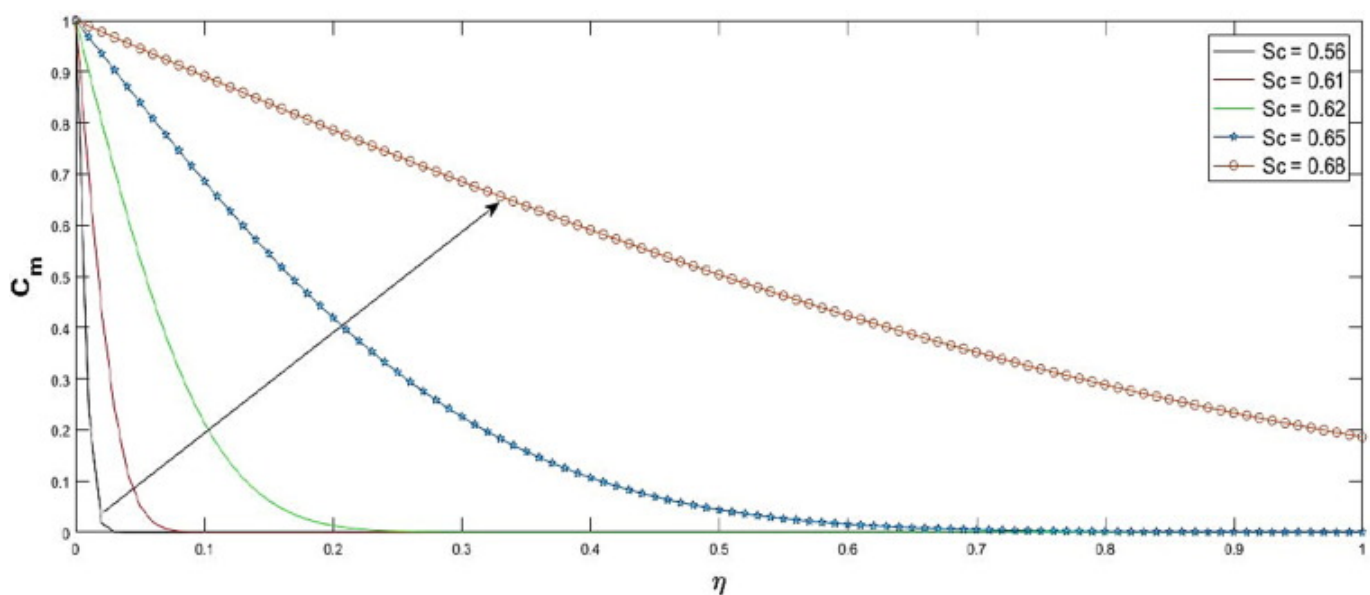
Download : Download high-res image (251KB)
Download : Download full-size image

Fig. 8. Variation in Concentration profile with respect to Schmidt number.

Chemical reaction parameter:

Fig. 9, Fig. 10 demonstrates that the Concentration disseminations are expanded enthusiastically concerned impact of different expanding Kr and time parameters. As a result of mass diffusion, fluid motion is accelerated. Arrhenius energy for chemical reactions. It's nonlinear impact. Many chemical reactions do not follow linear relationship. First-order chemical reactions means change of conc is directly proportional to concentration. We can consider exponential type.. contains nonlinear impact. Arrhenius function helps to increase the process molecule reaction. Higher assessment of the activation energy boundary deteriorates the altered Arrhenius work which pushes to produce the compound response in mucus fluid.
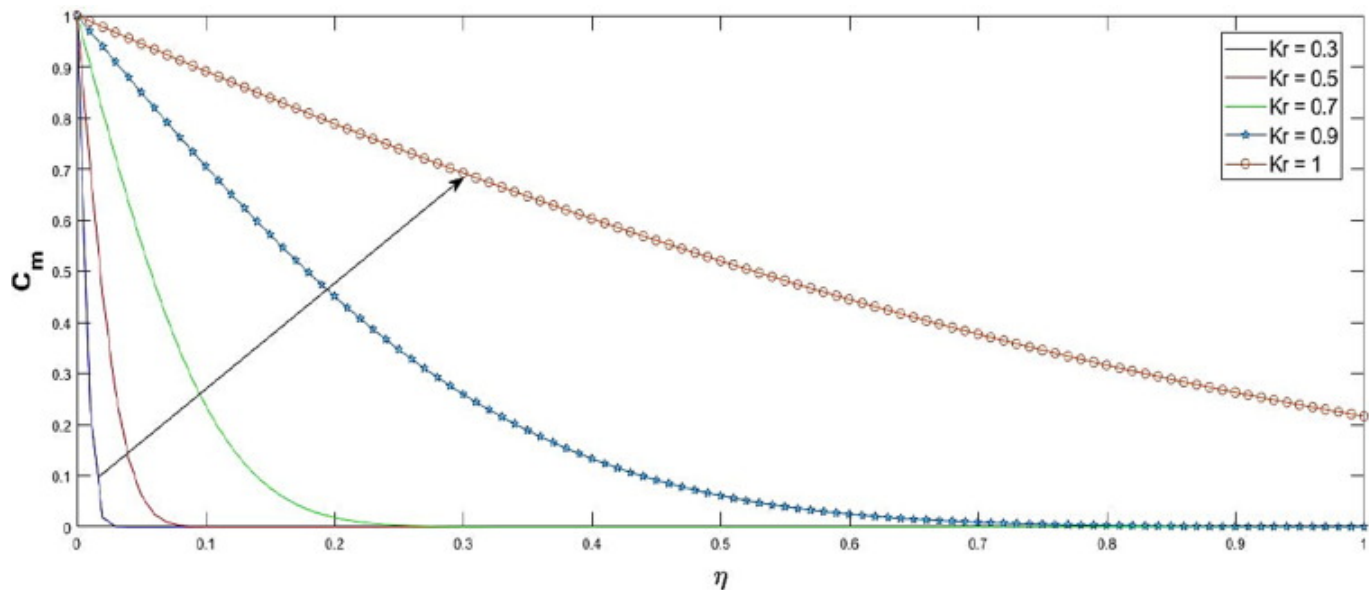
Fig. 9. Variation in Concentration profile with respect to Chemical reaction parameter.
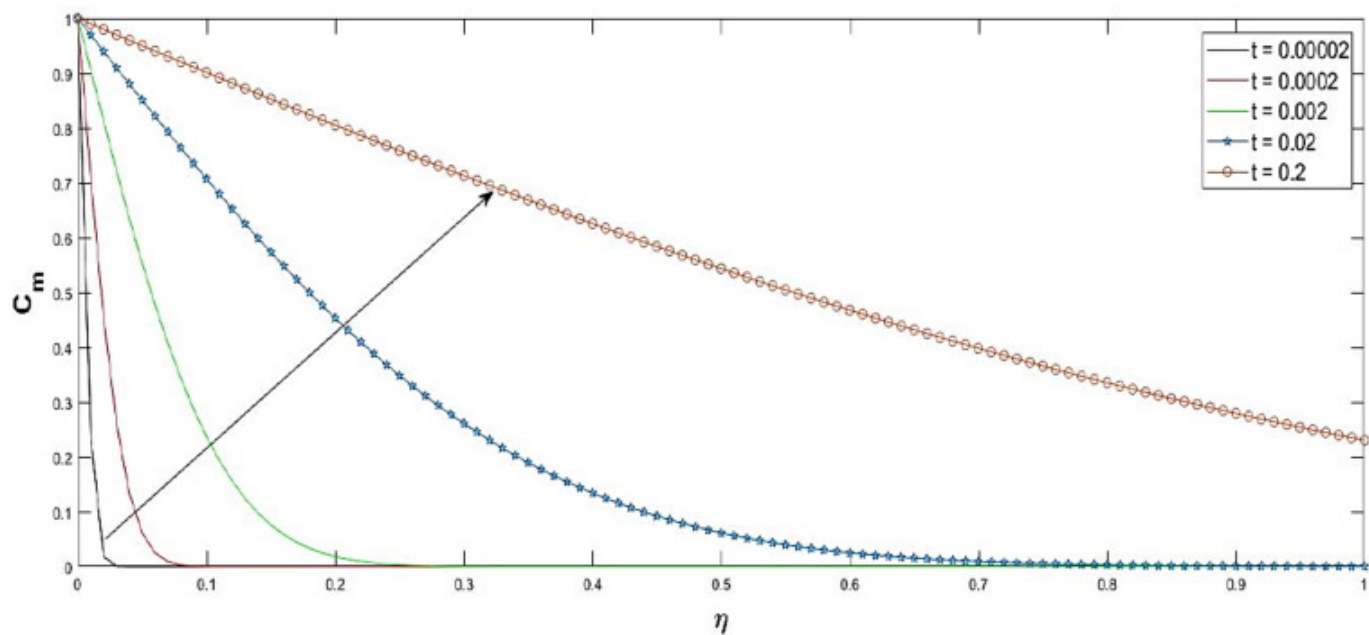
Fig. 10. Variation in Concentration profile with respect to time.

Nusselt Number:

Nusselt number increments with expanding upsides of Pr for both water $(Pr = 7.0)$ and air $(Pr = 0.71)$. It is likewise seen that Fig. 11 Nusselt number for water is greater than air. The

explanation is that little upsides of Pr are identical to expanding the warm strength and consequently heat can disperse away from the periciliary layer further quickly than higher upsides of Pr, thus the pace of heat exchange is diminished. Diffusion thermal effect, on the other hand, has the opposite effect on Nusselt number and temperature profile.
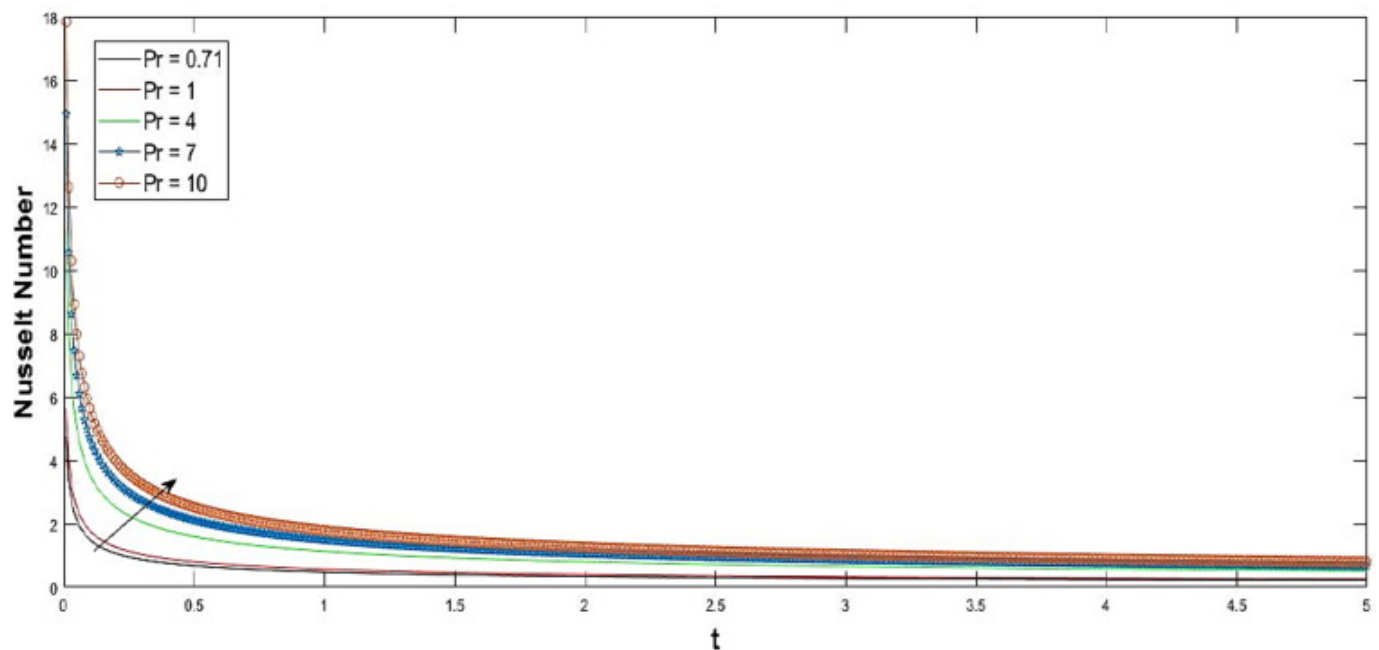
Fig. 11. Variation in Nusselt Number with respect to Prandtl Number.

Sherwood Number:

Fig. 12, Fig. 13, uncovers the Sherwood number expansion with the expanding upsides of Sc and Kr. The pseudo-diffusivity in the PCL is lower than the drug's molecular diffusivity, as indicated by Sh<1. This behavior may appear strange at the first glance when convection only amplifies mixing, therefore it's uncertain how the PCL's pseudo-diffusivity can be lower than the drug's molecular diffusivity. The appearance of cilia, on the other hand, presents barriers to the drug's unrestricted transport in the fluid, lessening apparent dispersion in the PCL.
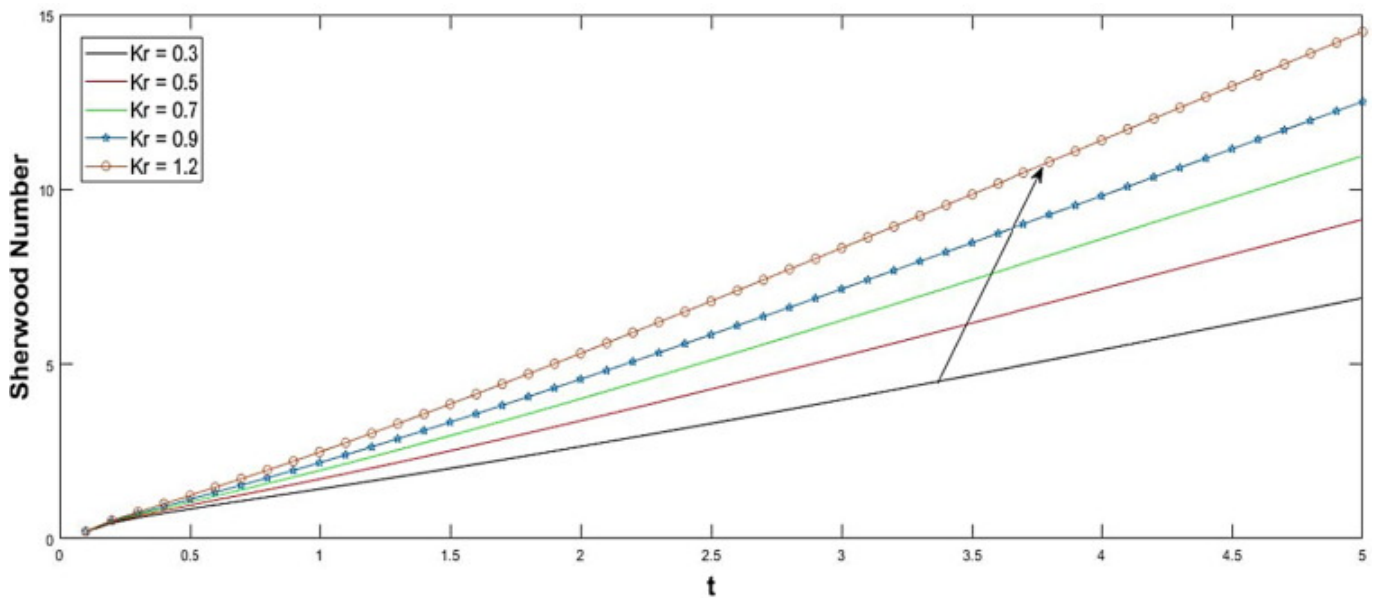
Fig. 12. Variation in Sherwood Number with respect to Chemical reaction parameter.
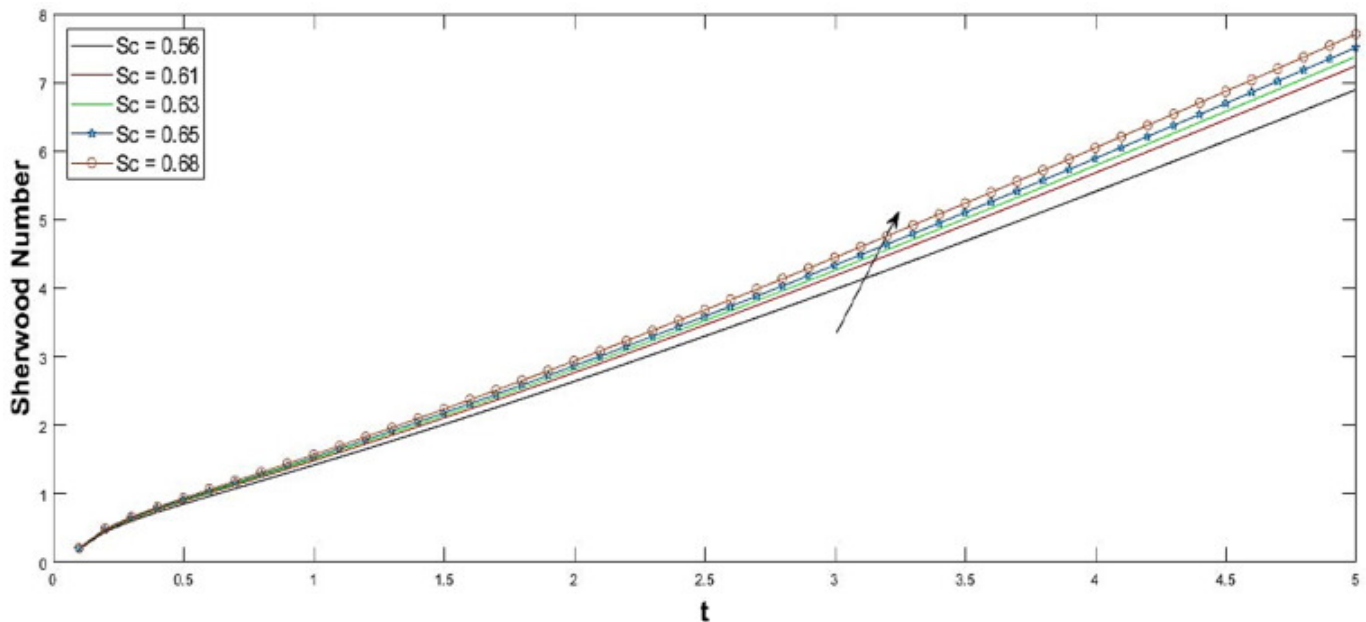
Fig. 13. Variation in Sherwood Number with respect to Schmidt Number.

Skin Friction:

The mathematical upsides of skin-friction τ are introduced in Fig. 14, Fig. 15 for Various Thermal &Mass Grashof Number. It is likewise seen that the skin-friction increments with expanding upsides of
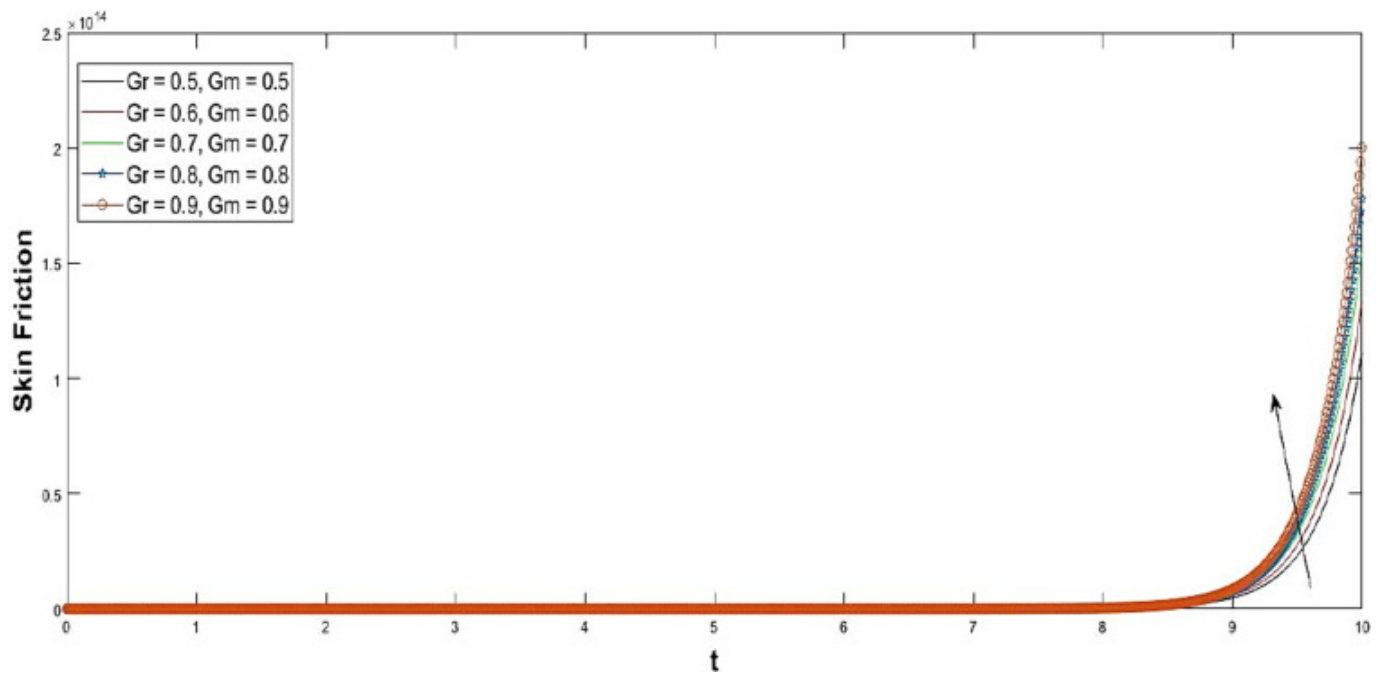
the Thermal & Mass Grashof Number.
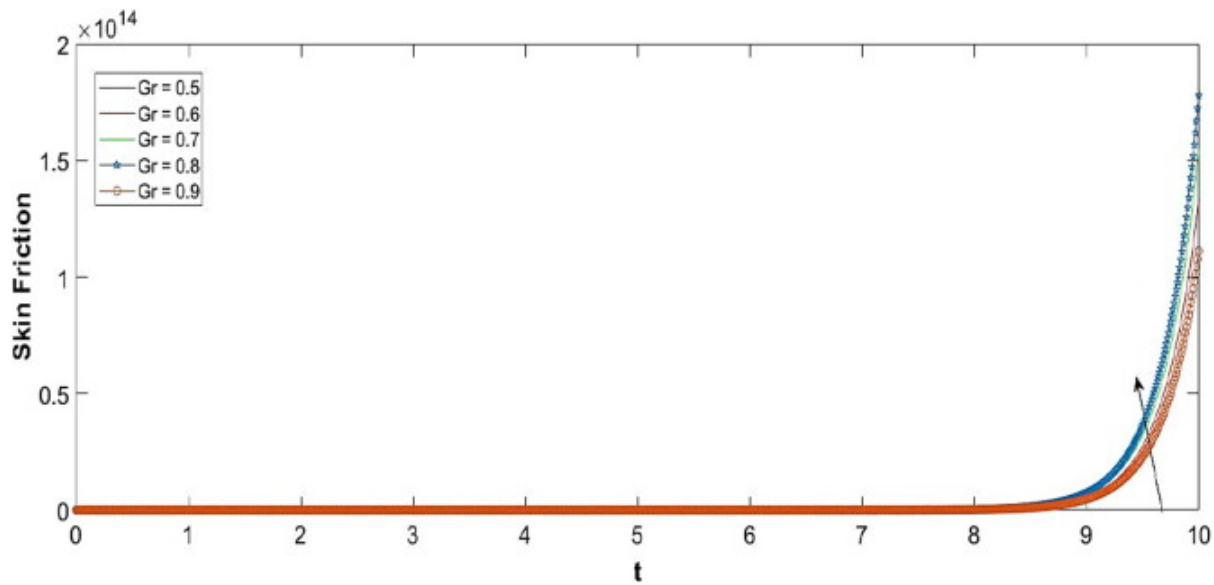
Fig. 14. Variation in skin friction with respect to Grashof Number.

Fig. 15. Variation in skin friction with respect to Mass Grashof Number.

5. Conclusion

The purpose of this study is to determine how the ciliated tissue affects the mucus layer. We looked into the role of cilia flexibility and mucus diffusivity at the beginning.

The development of mass transfer source exchange has significantly been hampered because of the exceptional epidemic of COVID-19 by [24]. The model can uncover the wind current and concentration dissemination inside the whole lungs. The CO_2 fixation was above required level in the lung wall, which is a lot higher than whatever is free from danger for human wellbeing. Which can't be tackled exclusively by clinical measurements and medication related research. The recent findings may have consequences for our knowledge of the lungmechanisms that cause severe disease and severe pulmonary syndrome in ciliopathies patients. The mucociliary becomes less effective for patients with primary pulmonary ciliary dyskinesia or the more prevalent form of acquired (secondary) ciliary dyskinesia since the cilia's function is affected or entirely suppressed. It also has crucial consequences for the speed with which medications and hazardous substances can reach the airway epithelium, as shown in this study.

The final reports of the review produce the accompanying outcomes:
- The force of the liquid stream dynamically improves the response of expanded Grashof numbers.

- The impact of expanding Porosity boundary eventually expanded the pace of velocity disseminations.

- Temperature field of the mucous gel is improved with developing Prandtl numbers. Thickness of the warm limit layer heightened when the Prandtl number expanded. Temperature angle increments step by step at the lung divider due to variation of the corresponding dimensionless parameters.

- The chemical diffusion of the mucus fluid layer increments with relating non-layered boundaries Sc, Kr and the time increments.

- Skin Friction

- Nusselt Number increases with expanding upsides of Pr.

- Sherwood Number increases with expanding upsides of Sc, Kr.

Future study will desire joining the vanishing model grew in this with trial estimations of the underlying size and speed of breathed out respiratory droplets. This access will serve to essentially propel how we might interpret COVID-19 transmission through respiratory discharges. Also, we believe that our results could help clinicians to superior evaluation and administer COVID-19 patients with Mucus transport.

Author contributions

All authors have read and agreed to the equal contribution of this manuscript.

Funding

<u>Institutional Review Board</u> Statement.

Not applicable.

Informed Consent Statement: Not applicable.

Declaration of Competing Interest

The authors declare that they have no known competing financial interests or personal relationships that could have appeared to influence the work reported in this paper.

Acknowledgments

Appendix A.

$$\eta = \frac{y}{2\sqrt{t}}, F = s + \sigma^2 + M, R = -ScKr + F, a = \frac{F}{1-Pr}, b = \frac{R}{1-Sc}$$

Recommended articles

Data Availability Statement:

Not applicable.

References

[1]   M. Ariane, S. Kassinos, S. Velaga, Alexiadis, A discrete multi-physics simulation of diffusive and convective mass transfer in boundary layers containing motile cilia in lungs. Comput. Biol. Med., 95 (2018) 34–42. <u>https://doi.org/10.1016/j.compbiomed.2018.01.010</u> ↗.

Google Scholar ↗

[2]   H. Sadaf, S. Nadeem

Fluid flow analysis of cilia beating in a curved channel in the presence of magnetic field and heat transfer

Can. J. Phys., 98 (2) (2020), pp. 191-197

CrossRef ↗   View in Scopus ↗   Google Scholar ↗

[3]   M.H. Kamel

Unsteady MHD convection through porous medium with combined heat and mass transfer with heat source/sink

Energy Convers. Manage., 42 (4) (2001), pp. 393-405, 10.1016/S0196-8904(00)00067-4 ↗

🗎 View PDF   View article   View in Scopus ↗   Google Scholar ↗

[4]   Kiskor Kumar Das

Diffusion thermo effect on an unsteady MHD free convective mass transfer flow past an accelerated vertical plate with chemical reaction and heat sink

Int. J. Appl. Eng. Res., 16 (5) (2021), pp. 393-399

View in Scopus ↗   Google Scholar ↗

[5]   M. Yao, L.u. Zhang, J. Ma, L. Zhou

On airborne transmission and control of SARS-Cov-2

Sci. Total Environ., 731 (2020), p. 139178, 10.1016/j.scitotenv.2020.139178 ↗

🗎 View PDF   View article   View in Scopus ↗   Google Scholar ↗

[6]   H. Khatun, S. Ahmed

Laplace analysis of periodic heat and mass transport on a parabolic started surface immersed in Darcian porous regime

Int. J. Eng. Res. Appl., 07 (04) (2017), pp. 09-17

CrossRef ↗   Google Scholar ↗

[7]   N.A. Kulkarni, C. Kleinstreuer

High-temperature effects on the mucus layers in a realistic human upper airway model

Int. J. Heat Mass Transfer, 163 (2020), p. 120467, 10.1016/j.ijheatmasstransfer.2020.120467 ↗

🗎 View PDF   View article   View in Scopus ↗   Google Scholar ↗

[8]   M. Nazeer, S. Saleem, F. Hussain, S. Iftikhar, A. Al-Qahtani

Mathematical modeling of bio-magnetic fluid bounded by ciliated walls of wavy channel incorporated with viscous dissipation: discarding mucus from lungs and blood streams

Int. Commun. Heat Mass Transfer, 124 (2021), p. 105274, 10.1016/j.icheatmasstransfer.2021.105274 ↗

🗎 View PDF   View article   View in Scopus ↗   Google Scholar ↗

[9]   M. Jayaweera, H. Perera, B. Gunawardana, J. Manatunge

Transmission of COVID-19 virus by droplets and aerosols: a critical review on the unresolved dichotomy

Environ. Res., 188 (2020), p. 109819, 10.1016/j.envres.2020.109819 ↗

🔲 View PDF   View article   View in Scopus ↗   Google Scholar ↗

[10]   R. Hirose, T. Nakaya, Y. Naito, T. Daidoji, R. Bandou, K. Inoue, O. Dohi, N. Yoshida, H. Konishi, Y. Itoh, H.F. Rosenberg

Situations leading to reduced effectiveness of current hand hygiene against infectious mucus from influenza virus-infected patients

mSphere, 4 (5) (2019), 10.1128/mSphere.00474-19 ↗

Google Scholar ↗

[11]   M. Zhang, J. Sun, B. Fricke, K. Nawaz, K. Gluesenkamp, B.o. Shen, J. Munk, X. Liu

A study on computational fluid dynamics modeling of a refrigerated container for COVID-19 vaccine distribution with experimental validation

Int. Commun. Heat Mass Transfer, 130 (2022), p. 105749, 10.1016/j.icheatmasstransfer.2021.105749 ↗

🔲 View PDF   View article   View in Scopus ↗   Google Scholar ↗

[12]   A. Riaz, A. Gul, I. Khan, K. Ramesh, S. Ullah Khan, D. Baleanu, K. Sooppy Nisar

Mathematical analysis of entropy generation in the flow of viscoelastic nanofluid through an annular region of two asymmetric annuli having flexible surfaces

Coatings, 10 (2020), p. 213, 10.3390/coatings10030213 ↗

View in Scopus ↗   Google Scholar ↗

[13]   Rajneesh Bhardwaja, Amit Agrawala, Tailoring surface wettability to reduce chances of infection of COVID-19 by a respiratory droplet and to improve the effectiveness of personal protection equipment, Phys. Fluids 32 (2020) 081702, https://doi.org/10.1063/5.0020249 ↗.

Google Scholar ↗

[14]   H.S. Gaikwad, P. Baghel, R. Sarma, P.K. Monda

Transport of neutral solutes in a viscoelastic solvent through a porous microchannel

Phys. Fluids, 31 (2019), Article 022006, 10.1063/1.5064777 ↗

View in Scopus ↗   Google Scholar ↗

[15]   J.-M. Heydel, F. Menetrier, C. Belloir, F. Canon, P. Faure, F. Lirussi, E. Chavanne, J.-M. Saliou, Y. Artur, M.-C. Canivenc-Lavier, L. Briand, F. Neiers, F. Rodrigues-Lima

Characterization of rat glutathione transferases in olfactory epithelium and mucus

PLoS ONE, 14 (7) (2019), p. e0220259

CrossRef ↗   View in Scopus ↗   Google Scholar ↗

[16]   W. Liu, F. Mo, G. Jiang, H. Liang, C. Ma, T. Li, L. Zhang, L. Xiong, G. Mariottini, J. Zhang, L. Xiao

Stress-induced mucus secretion and its composition by a combination of proteomics and metabolomics of the Jellyfish Aurelia coerulea

Mar. Drugs, 16 (9) (2018), p. 341, 10.3390/md16090341 ↗

Google Scholar ↗

[17] C. Wang, D.B. Collins, C. Arata, A.H. Goldstein, J.M. Mattila, D.K. Farmer, L. Ampollini, P.F. DeCarlo, A. Novoselac, M.E. Vance, W.W. Nazaroff, J.P.D. Abbatt

Surface reservoirs dominate dynamic gas-surface partitioning of many indoor air constituents

Sci. Adv., 6 (8) (2020), 10.1126/sciadv.aay8973 ↗

Google Scholar ↗

[18] K.V. Chandra Sekhar, Laplace transform solution of unsteady MHD jeffry fluid flow past vertically inclined porous plate, Front. Heat Mass Transfer 16 (2021) 10, https://DOI:10.5098/hmt.16.10 ↗.

Google Scholar ↗

[19] V.-G. Peppa, E.I. Solenov, I. Kalomenidis, I. Tsilioni, K.I. Gourgoulianis, C. Hatzoglou, S.G. Zarogiannis

Pleural effusion osmolality correlation with pH and glucose level of pleural fluid and its effects on the pleural membrane permeability

Respir. Physiol. Neurobiol., 285 (2021), p. 103581, 10.1016/j.resp.2020.103581 ↗

🅿 View PDF   View article   View in Scopus ↗   Google Scholar ↗

[20] B, Mukherjee, N, Prasad, Effect of radiation and porosity parameter on hydromagnetic flow due to exponentially stretching sheet in a porous media. Int. J. Eng. Sci. Technol. 6(1) (2014) 58–70, https://doi.org/10.4314/ijest.v6i1.7 ↗.

Google Scholar ↗

[21] D. Wu, M.H. Tawhai, E.A. Hoffman, C.-L. Lin

A numerical study of heat and water vapor transfer in MDCT-based human airway models

Ann. Biomed. Eng., 42 (10) (2014), pp. 2117-2131

CrossRef ↗   View in Scopus ↗   Google Scholar ↗

[22] Mehdi Stitia, Guilaume, Castanet, Andrew, Corber, Marcus, Alden, Edouard, Berrocal, Transition from saliva droplets to solid aerosols in the context of COVID-19 spreading, Environ. Res. 204(Part B) (2022) 112072, https://doi.org/10.1016/j.envres.2021.112072 ↗.

Google Scholar ↗

[23] T. Padmavathi, S. Senthamilselvi

Effect of hartmann number on natural convection of pleural effusion

Turk. J. Comput. Math. Educ., 12 (2021), pp. 5672-5681

Google Scholar ↗

[24] T. Padmavathi, S. Senthamil Selvi, S.S. Santra, R. Ali, V. Govindan, S. Noeiaghdam, J.J. Nieto

Free and Forced Convective Flow in Pleural Fluid with Effect of Injection between Different Permeable Regions

Coatings, 11 (1313) (2021), 10.3390/coatings11111313 ↗

Google Scholar ↗

[25] B.M.J. Rana, S.M. Arifuzzaman, S.k. Reza-E-Rabbi, S.F. Ahmed, M.d. Shakhaoath Khan

Energy and magnetic flow analysis of Williamson micropolar nanofluid through stretching sheet

Int. J. Heat Technol., 37 (2) (2019), pp. 487-496, 10.18280/ijht.370215 ↗

View in Scopus ↗   Google Scholar ↗

[26] B.M.J. Rana, S.M. Arifuzzaman, S. Islam, S.k. Reza-E-Rabbi, A. Al-Mamun, M. Mazumder, K.C. Roy, M.S. Khan

Swimming of microbes in blood flow of nano-bioconvective Williamson fluid

Therm. Sci. Eng. Progr., 25 (2021), p. 101018, 10.1016/j.tsep.2021.101018 ↗

📄 View PDF   View article   View in Scopus ↗   Google Scholar ↗

[27] R. Robinot, M. Hubert, G.D. de Melo, F. Lazarini, T. Bruel, N. Smith, S. Levallois, F. Larrous, J. Fernandes, S. Gellenoncourt, S. Rigaud, O. Gorgette, C. Thouvenot, C. Trébeau, A. Mallet, G. Duménil, S. Gobaa, R. Etournay, P.-M. Lledo, M. Lecuit, H. Bourhy, D. Duffy, V. Michel, O. Schwartz, L.A. Chakrabarti

SARS-CoV-2 infection induces the dedifferentiation of multiciliated cells and impairs mucociliary clearance

Nat. Commun., 12 (1) (2021), 10.1038/s41467-021-24521-x ↗

Google Scholar ↗

[28] M. Nawaz, S. Rana, I.H. Qureshi, T. Hayat

Three-dimensional heat transfer in the mixture of nanoparticles and micropolar MHD plasma with Hall and ion slip effects

AIP Adv., 8 (10) (2018), p. 105109, 10.1063/1.5050670 ↗

View in Scopus ↗   Google Scholar ↗

[29] N. Gajjela, M. Garvandha

Impacts of variable thermal conductivity and mixed convective stagnation-point flow in a couple stress nanofluid with viscous heating and heat source

Heat Transfer., 49 (6) (2020), pp. 3630-3650

CrossRef ↗   Google Scholar ↗

[30] N. Gajjela, R. Nandkeolyar

Investigating the magnetohydrodynamic flow of a couple stress dusty fluid along a stretching sheet in the presence of viscous dissipation and suction

Heat Transfer., 50 (3) (2021), pp. 2709-2724

CrossRef ↗   View in Scopus ↗   Google Scholar ↗

[31]   A. Matta, N. Gajjela

Order of chemical reaction and convective boundary condition effects on micropolar fluid flow over a stretching sheet

AIP Adv., 8 (11) (2018), p. 115212, 10.1063/1.5053445 ↗

View in Scopus ↗   Google Scholar ↗

[32]   G, Nagaraju, A. Matta, K. Kaladhar, Effects of chemical reaction and thermal radiation on heat generated stretching sheet in a couple stress fluid flow. Front. Heat Mass Transf. 7(11) (2016) 1–5. ISSN 2151-8629.

Google Scholar ↗

Cited by (9)

Computational analysis of heat and mass transfer flow of wall jet hybrid nanofluid with irregular heat source/sink effects and waste discharge concentration

2023, Journal of Magnetism and Magnetic Materials

Show abstract ⌄

A case study for heat and mass transfer of viscous fluid flow in double layer due to ciliated channel

2023, Case Studies in Thermal Engineering

Show abstract ⌄

Performance of magnetic dipole contribution on ferromagnetic non-Newtonian radiative MHD blood flow: An application of biotechnology and medical sciences

2023, Heliyon

Show abstract ⌄

Arrhenius activation energy of tangent hyperbolic nanofluid over a cone with radiation absorption

2022, Results in Engineering

> *Citation Excerpt :*
>
> …Formation of entropy during nanofluid flow onto a thin needle was discussed by Afridi et al. [15]. More studies on fluid and nanofluid can be found in Refs. [31–44]. The term "activation energy" refers to the lower energy amount that is necessary to initiate the process of a chemical reaction.…

Show abstract ⌄

[A chemical engineering application on hyperbolic tangent flow examination about sphere with Brownian motion and thermo phoresis effects using BVP5C](#)

2022, Case Studies in Thermal Engineering

> *Citation Excerpt :*
>
> …The natural nano fluid convective BLF through a surface has been explored by ([2–4]) using the Buongiorno model. More discussions on fluid and nanofluid flow can be found in Refs. [18–25,34,35]. In virtue of their wide range of industrial uses, non-Newtonian fluids' heat transfer and BLF have recently attracted the attention of many scientists.…

Show abstract ∨

[Analysis of a Ferromagnetic Nanofluid Saturating a Porous Medium with Nield's Boundary Conditions ↗](#)

2023, Mathematics

> ⟩ View all citing articles on Scopus ↗

Peer review under responsibility of Faculty of Engineering, Alexandria University.

ELSEVIER

ℛ RELX™